Abstract

Investigating a Locomotor Neuron that Makes a Potential Sensory Cilium Lying over the *C. elegans* Egg-laying Apparatus, Designing an Accessible System for Neuron Identifications, and Advancing Imaging and Modeling in the Egg-laying System

Nakeirah Christie

2022

The neural circuit for *Caenorhabditis elegans* egg laying has been studied intensively for decades, yet its known components cannot account for how egg laying and locomotion behaviors are coordinated. In my graduate work within the Koelle lab, I worked to further complete that model circuit. The first half of this dissertation covers my work on the PVP neurons. I discovered that the PVP neuron pair, which has previously been implicated in locomotion, makes previously-undescribed branches that terminate in large wing-shaped endings directly over the egg-laying apparatus. The PVP wing structures occur only in hermaphrodites and develop during the L4 larval stage when the egg-laying system also develops. The PVP wing is located at the junction between the uterus and the vulva, adjacent to neurons that control egg laying, and is surrounded by cells that express a glial marker. This latter result suggests that the PVP structure may be cilia; however, the structures are not absent as other cilia are in *cilialess* mutants. Moreover, the sensitivity of the PVPs to expression of transgenes prevented recording or manipulating PVP activity to determine its functional roles. The second half of this dissertation describes microscopy, data analysis, and modeling work that significantly contributed to several additional projects in the Koelle lab, including the use of a new tool to identify individual neurons and better models to communicate expression data of GPCRS.

Investigating a Locomotor Neuron that Makes a Potential Sensory Cilium Lying over the *C. elegans* Egg-laying Apparatus, Designing an Accessible System for Neuron Identifications, and Advancing Imaging and Modeling in the Egg-laying System

A Dissertation

Presented to the Faculty of the Graduate School

Of

Yale University

In Candidacy for the Degree of

Doctor of Philosophy

By

Nakeirah T.M. Christie

Dissertation Director: Michael Koelle

December 2022

Table of Contents

List of Figures

List of Tables

Acknowledgements

I am very grateful for the support I have received over the course of my graduate work, both professionally and personally. I first must thank my advisor, Dr. Michael Koelle, who showed me immense kindness, encouragement, and support when I found myself as a third year whose previous PI did not earn tenure and was unexpectedly leaving Yale—leaving me without a lab or infrastructure to continue my graduate work. Thanks to Michael, I was able to continue to my graduate work and engage in my passion for science. I am also exceedingly grateful to my committee members Drs. Christian Schlieker and Valerie Reinke, who have been endlessly patient, supportive, and reassuring—often fitting me in at short notice—through all the low-points and struggles that are built into graduate school. I'd also to thank Dr. Anne Hart for being my outside reader and taking time out of a busy schedule to evaluate my work. Thank you to Dr. Richard Ikegami for supplying the promoter without which I could not have studied the PVP neuron, and to Agustin Porras (Gus) for gifting me the *odr-1p::RFP* plasmid. I am also grateful for the NIH F31 award and the Training Program in Genetics for funding my work throughout graduate school. Furthermore, I am thankful to my labmates for all their thoughtful discussion, input, and comradery during long days in the lab. I am also thankful for my family, friends, loved ones, and neighbors who were nothing but inspiring, encouraging, and caring. Thank you to my mother for our long phone calls and my sister for her sense of humor; Tanner, Adan, and Kathy for introducing me to some of the most bizarre reality TV; Vincent for exposing me to Drumcore Marching Band competitions; Allison, Jen, Sam, and Ben for playing Dungeons and Dragons every week and building a whole world with me; Halie for cozy pick-me-ups and great conversation; Andrew for the good chats and shared stories; Tim for providing a home away from home (even if it did come with endless teasing); and Michiyo, Koko, Masa, and Shino for being my second family in New Haven. And thank you to Tony for supporting me through it all.

1. Chapter 1: The PVP

N.B. This chapter is a modified copy of the paper *"A neuron that regulates locomotion makes a potential sensory cilium lying over the C. elegans egg-laying apparatus"* that was submitted to the journal G3 on the 17th of September, 2022.

Figure legends have been modified to follow the outline format of the thesis (e.g., Figure 1 in the manuscript is now Figure 1-1) and tables in the supplementary file have been supplied.

A neuron that regulates locomotion makes a potential sensory cilium lying over the C. elegans egg-laying apparatus

Nakeirah T.M. Christie and Michael R. Koelle

Department of Molecular Biophysics and Biochemistry, Yale University, New Haven, CT 06520 USA

ORCID IDs: 0000-0001-9486-8481 (M.R.K.), 0000-0002-4071-7423 (N.T.M.C.)

KEYWORDS

C. elegans, egg laying, neural circuit, sensory cilium, glial cell

Abstract

The neural circuit for *C. elegans* egg laying has been studied intensively for decades, yet it is not clear that its known components can account for how egg-laying and locomotion behaviors are coordinated. We found that the two PVP neurons, which release neuropeptides that promote roaming locomotion, make previously-undescribed branches that terminate in large wing-shaped endings directly over the egg-laying apparatus. The PVP branches occur in hermaphrodites but not males and develop during the L4 larval stage when the egg-laying system also develops. The PVP wing is located at the junction between the uterus and the vulva, adjacent to neurons that control egg laying, and surrounded by cells that we found label with a glial marker. The morphology of the PVP wing and its envelopment within possible glial cells are consistent with the hypothesis that the PVP wing is a sensory cilium. Although PVP is reported to express sensory receptor homologs, we have been unable to detect PVP expression of more specific markers of neural cilia, and we have also not detected strong PVP defects in the *daf-19* mutant, which does show defects in known neural cilia. The PVPs are extraordinarily sensitive to expression of multicopy array transgenes, which cause developmental and possibly functional defects in these neurons. Thus, the intriguing hypothesis that PVP is a sensory neuron that might coordinate egg laying and locomotion will remain speculative until better methods to manipulate PVP can be developed.

Introduction

Neural circuits are functional units in the brain consisting of groups of neurons that respond to stimuli and signal to each other to produce dynamic patterns of activity (Bargmann and Marder 2013). Defects at the level of neural circuit function are thought to result in a variety of highly prevalent mental health problems. For example, it is estimated that over a fifth of U.S. adults will experience a mood disorder at some point in their life (Kessler et al. 2005). It remains difficult to understand how abnormalities in neural circuits arise and result in such disorders because the mechanisms that underlie neural circuit function remain poorly understood. Currently there is no neural circuit in any organism in which it is understood how the complete set of signals among the all the neurons involved produces the dynamic pattern of activity that carries out the function of the circuit.

One approach to advance our understanding of neural circuits is to intensively study small neural circuits of genetically-tractable invertebrates, with the hope that deeply understanding a few such model circuits will reveal general principles by which all neural circuits operate. With only 302 neurons, the nematode *C. elegans* offers the opportunity to completely describe all the components of individual neural circuits. Alongside a physical connectome which traces each neuron's processes and the ~7000 physical synapses they make (Albertson and Thompson 1976; White et al. 1986; Xu et al. 2013), there is also a detailed map of which neurons release what neurotransmitter (Serrano-Saiz et al. 2013; Pereira et al. 2015; Gendrel et al. 2016).

Within *C. elegans*, one of the best-characterized model neural circuits is the egg-laying circuit. Not only does it have ~12 neurons and 16 muscle cells, but it also has a simple output (i.e., an egg being laid), ideal for quantitative behavioral analysis (Schafer 2005). Despite the fact that each neuron known to be part of the circuit has had its activities and functions investigated in detail (Collins and Koelle 2013; Collins et al. 2016; Brewer et al. 2019;

Kopchock et al. 2021), there remain behaviors produced by this circuit that cannot be explained by these neurons. For instance, previous research shows that the presence of eggs in the uterus stimulates activity of the egg laying circuit, but no mechanism for the circuit to sense these eggs is known (Collins et al. 2016). Eggs tend to be laid at a particular phase of locomotor body bends (Collins et al. 2016), and animals do not lay eggs when immobilized, but the neural mechanisms responsible coordinating egg laying locomotion behavior remain unknown. Additionally, a variety of factors in the environment (e.g., the presence of food) appear to regulate egg laying (Dong et al. 2000), but the mechanisms used to sense these factors and relay their presence to the egg-laying circuit remain unclear. These unexplained phenomena imply that there are likely additional cells that regulate activity of the currently-recognized components of the egg-laying circuit. As long as these additional components of the egg-laying circuit remain unknown, it will not be possible to obtain a full mechanistic understanding of how activity of the egg-laying circuit is controlled, limiting the utility of the egg-laying circuit as a model for understanding neural circuit function and dysfunction in general. In this work, we have characterized a pair of PVP neurons that may constitute a new component of the *C. elegans* egg-laying system.

Materials and Methods

Strains and culture

C. elegans strains were cultured at 20°C on NGM agar plates with *E. coli* strain OP50 as a nutrient source (Brenner 1974). Genetic crosses were maintained by standard methods (Fay 2013). Extrachromosomal-array transgenic strains were generated through standard microinjection (Evans 2006). Chromosomal integration of such transgenes was performed via UV/TMP mutagenesis (Fernandez et al. 2020), and integrated strains were backcrossed to N2 to remove background mutations as indicated in Table 1.

Transgenes

The supplemental material describes all transgenes used in this study. A GFP reporter plasmid, pEXP294, expressed exclusively in PVP within L4 and adult animals was a gift from Richard Ikegami. In this plasmid, the promoter used (*PVPp*) is derived from 699 bp of the *C. elegans* dystroglycan (*dgn-1*) gene, (primers F:catggggatccggacaatgagaatgag; R:gccttttgtcttatatacatttttttagaccgttcaca). To increase expression of GFP the Syn21 translational enhancer and AcNPV p10 3'UTR were utilized (Pfeiffer et al. 2012). The *PVPp::GFP* transgene used to visualize PVP also co-expressed a histamine-gated chloride channel in PVP, although histamine was not applied to the animals to activate this channel in any experiments shown in this article. To express other proteins in PVP, we cloned the *dgn-1* promoter and AcNPV p10 3'UTR into the vector pPD49.26 (from the Andrew Fire plasmid kit, Addgene Kit #1000000001) to generate plasmid pNTC2, wherein we were able to drop coding sequences of interest into the multiple cloning site downstream of the promoter along with the Syn21 translational enhancer to express proteins of interest in PVP (Table 2).

Confocal Imaging

Animals were mounted on agarose pads on microscope slides Superfrost (ThermoFisher Scientific) and a 22x22-1 microscope cover glass (ThermoFisher Scientific). The 2% agarose pads contained 25 mM of sodium azide (Sigma Aldrich) and 120 mM of 60% w/v iodixanol (Optiprep; Sigma Millipore) to reduce refractive index mismatch (Boothe et al. 2017). Images were acquired on an LSM 880 using a $40x$ water immersion objective (Carl Zeiss), with either standard confocal imaging, spectral imaging (lambda stacking) to filter out autofluorescence, or fast Airyscan SR mode, as indicated. Animals were imaged within 2 hours of mounting, to avoid desiccation.

Developmental Time Course

Animals carrying transgenes that label PVP were picked on a dissecting microscope at various developmental points within the L4 larval stage and mounted for confocal imaging, recording both fluorescent and brightfield images. Using the brightfield image, animals were sub-staged according to vulval morphology (Mok et al. 2015), binning L4.0-L4.2 as "early L4", L4.3-L4.5 as "mid-L4", and L4.6-L4.9 as "late L4."

Strains, Plasmids, and Transgenes

Table 1-1: Strain and n-number information by experiment

Figure	**Strain Used**	**Question**	***n*-number**
1-1B-C	• LX2622 *(PVPp::HisCl/PVPp::GFP*)	Are the PVP wing structures sex-specific?	• *n* = 15 adult hermaphrodites • *n* = 15 adult males
1D-1G	• LX2622 *(PVPp::HisCl/PVPp::GFP*)	What do these wing shaped structures look like?	• *n* = 20 adult hermaphrodites
1-2	• LX2406 *(PVPp::GFP)* • AML5 *(odr-2p::GFP)* • LX2360 *(dop-6::GFP)*	Is the PVP wing structure an artefact?	• *n* = 20 adult LX2406 hermaphrodites • *n* = 20 adult AML5 hermaphrodites • *n* = 20 adult LX2360 hermaphrodites
1-3	• LX2622 *(PVPp::HisCL/PVPp::GFP*) • AML5 *(odr-2p::GFP)* • *(ocr-3b::GFP)*	Is the wing structure being affected by transgene expression?	• *n* = 20 LX2622 *(PVPp::HisCl/PVP::GFP)* • *n* = 15 AML5 *(ocr-3b::GFP)* • *n* = 15 *ocr-3b::GFP*

1-4	• LX2682 (*PVPp::HisCl*/*PVPp::GFP* ; *ajm-1::mCh*)	When does the PVP wing structure develop?	• *n* = 10 early L4 animals • *n* = 10 mid L4 animals • *n* = 10 late L4 animals
1-5	• LX2681 (*PVPp::HisCl*/*PVPp::GFP* ; *ida-1p::mCh*) • LX2682 (*PVPp::HisCl*/*PVPp::GFP* ; *ajm-1::mCh*)	Where does the PVP wing structure lie, when dorsal, compared with known participants of the egg-laying system?	• *n* = 20 adult LX2681 hermaphrodites • *n* = 20 adult LX2682 hermaphrodites
1-6	• LX2448 (*daf-12(sa204) ; PVPp::GFP*/*odr-1p::RFP*) • LX2489 (*daf-12(sa204) ; daf-19(m86) PVPp::GFP*/*odr-1p::RFP*) • *mir-228p::GFP X PVPp::mCh* • *mir-228p::GFP X ajm-1::mCh*	Does the PVP wing structure behave the same way as other cilia?	• *n* = 10 adult LX2448 hermaphrodites • *n* =14 adult LX2489 hermaphrodites • *n* = 20 *mir-228p::GFP X PVPp::mCh* adult hermaphrodites • *n = mir-228p::GFP X ajm-1::mCh adult hermaphrodites*

Table 1-2: Strains Used

Strain	**Genotype**	**Features**	**Out-crossed**	**Used in figure(s):**	**Source**
AML5	*otIs355* IV; *kyIs51*	The *kyIs51* transgene expresses cytoplasmic GFP from the *odr-2* promoter in neurons including PVP, AIZ, AIB, SIAV, AVG, RIV, ASG and IL2 neurons. The *otIs355* transgene labels neuronal nuclei with mCherry.	N/A	1-2,1-3	Nguyen et al., 2016
LX2360	*vsIs241*	Integrated multicopy array of transgene expressing *dop-6::GFP.* Note that this is a fosmid containing the *dop-6* GPCR tagged with GFP and not a promoter::GFP fusion.	2x	1-2,3	Fernandez et al., 2020
LX2406	*vsEx894*	Extrachromosomal multicopy array transgene of *PVPp::GFP.*	N/A	1-2	This study
LX2446	*daf-12(sa204)* X; *vsEx916*	*daf-12* ciliated control animals expressing mCherry in AWC/AWB neurons (*odr-1p::RFP)* and GFP in the PVP.	N/A	1-6	This study
LX2449	*vsEx918*	Animals carry an extrachromosomal *PVPp*::*mCherry* transgene. This produces punctate red fluorescence in the PVPs and often makes the PVP neurons appear unhealthy.	N/A	1-6	This study

LX2478	*lin-15(n765ts) X; vsIs269*	Carries a chromosomally-integrated transgene that includes pBR1 (the *ida-1p::RFP* plasmid) and pL15EK (rescues the *lin-15* multi-vulva phenotype).	2x	1-5	This study
LX2489	*daf-19(m86) II; daf-12(sa204) X; vsEx927*	*daf-12; daf-19* animals with extrachromosomal transgene expressing mCherry in AWC/AWB neurons (*odr-1p::RFP*) and GFP in the PVP. The *daf-19* mutation disrupts most ciliated structures, while the *daf-12* mutation suppresses the lethality of the *daf-19* mutation.	N/A	1-6	This study
LX2562	*mjIs15*	Carries the chromosomally-integrated *ajm-1::mCherry* transgene that labels the apical junctions of epithelial cells.	2x	1-4,5,6	This study
LX2622	*lin-15(n765ts) X; vsIs280*	Carries a chromosomally integrated transgene with that includes plasmids pNTC6 (*PVPp::HisCl*), pL15EK (rescues the *lin-15* phenotype), and pEXP294 (*PVPp::GFP*).	4x	1-1,2,3	This study
LX2681	*lin-15(n765ts) X ; vsIs280; vsIs269*	Crossed LX2622 and LX2478 to see *PVPp::GFP* in the context of *ida-1p::mCh*.	*vsIs269* 1x outcrossed; *vsIs280* 5x	1-5	This study

			outcrossed		
LX2682	*lin-15(n765ts) X; vsIs280; mjIs15*	Crossed LX2622 and LX2562 to see *PVPp::GFP* in the context of *ajm-1p::mCherry*.	*vsIs269* 1x outcrossed; *mjIs* 5x outcrossed	1-4,5	This study
VT1485	*unc-119(ed3) III; maIs188*	"Pan-glial" marker [*mir-228p::GFP* + *unc-119*(+)] labeling glial cells with GFP.	N/A	1-6	Martinez et al., 2008

Table 1-3: Mutations and Transgenes Used in this Study

Allele	**Relevant features**	**For transgenes constructed in this study: injection components**	**Source**
daf-12(sa204) X	Dauer defective. Suppresses dauer-constitutive phenotype of *daf-19.*	N/A	Swoboda et al., 2000
daf-19(m86) II	Dauer constitutive, disrupts most known cilia structures.	N/A	Riddle et al., 1981
kyIs51	Cytoplasmic GFP expressed from the *odr-2b* promoter in neurons including PVP, AIZ, AIB, SIAV, AVG, RIV, ASG and IL2.	N/A	Nguyen et al., 2016
lin-15(n765ts) X	Temperature-sensitive multi-vulva phenotype. Used in strains that are recipients for transgene injections since it is rescued by the pL15EK plasmid, carrying a wild-type copy of *lin-15.*	N/A	Clark et al., 1994
maIs188	Chromosomally integrated transgene: [*mir-228p::GFP* + *unc-119*(+)]. Used as a pan-neuronal GFP marker.	N/A	Martinez et al., 2008
mjIs15	Marks apical junctions of epithelial cells.	N/A	Lehrbach et al., 2009
otIs355 IV	Pan-neuronal nuclear red fluorescent protein expression.	N/A	Nguyen et al., 2016

unc-119(ed3) III	Used in strains that are recipients for transgene injections - rescued by an *unc-119(+)* plasmid.	N/A	Maduro and Pilgrim, 1995
vsEx894	Expresses GFP in the PVPs. PVP specific at L4 and adults.	See methods on (transgenes)	This study
vsEx916	Expresses bright mCherry in the AWC and AWB sensory neurons; expresses GFP in PVP.	*odr-1p::RFP* at 25ng/µL, digested *E. coli* DH5a genomic DNA at 25ng/µL and plasmid pExP294 at 75ng/µL.	This study
vsEx918	Expresses mCherry in PVP.	pL15EK at 50ng/µL, digested DH5a genomic DNA at 25ng/µL, and pNTC3 at 50ng/µL.	This study
vsEx927	Bright mCherry labeling of AWC/AWB sensory neurons in the head; GFP labels PVP neurons.	*odr-1p::RFP* at 25ng/µL, digested *E. coli* DH5a genomic DNA at 25ng/µL, and	This study

		pExP294 at 75ng/µL	
vsIs241	Integrated array of vsEx874 expressing *dop-6::GFP*. LX2352 [*lin-15(n765ts)* X; *vsEx874*] animals were treated with UV/TMP and screened for integration. Note that this is the *dop-6* fosmid tagged with GFP and not a promoter::GFP fusion	*dop-6::GFP* at 60ng/µL, pL15EK at 50ng/µL, DH5α genomic DNA at 25ng/µL	Fernandez et al., 2020
vsIs269	Chromosomally integrated *ida-1::mCh* transgene. LX2471 [*lin-15(n765ts) X; vsEx928*] animals were treated with UV/TMP and screened for integration.	pBR1 at 20ng/µL, PLI5EK at 50ng/µL, digested *E. coli* DH5 alpha genomic DNA at 25ng/µL	This study
vsIs280	Integrated *PVPp::HisCl/PVPp::GFP*. Animals were treated with UV/TMP and screened for integration.	pNTC6 (*pDGN1::HisCl1*) at 50ng/µL, pExP294 (*pDGN1::GFP*) at 50ng/µL, pL15EK at 50ng/µL, digested *E. coli* DH5a genomic	This study

		DNA at 25ng/µL	

Table 1-4: Plasmids Used In this Study

Plasmid Name	**Features**	**Construction**	**Source**
pODR-1::RFP	Contains *odr-1p::RFP* marker.		Gift from Colon-Ramos lab
pL15EK	Contains a wild-type copy of the *lin-15* gene. Used as a co-injection marker to rescue the lin-15 phenotype.		Clark et al., 1994
pEXP294	Expression of GFP specifically in PVP neurons. A fragment of the *dgn-1* promoter driving GFP with *syn21* translational enhancer and ACPVN 3' UTR.	Gateway cloning	A gift from Richard Ikegami
pNTC1	"PVPp" promoter inserted into Andy Fire Vector pPD49.26.	The dgn-1 promoter fragment from pEXP294 were amplified using primers TACGCCAAGCTTcatggggatccggac and GTCGACCTGCAGtgtgaacggtctaaaaaaaatg with New England Biolabs Phusion	This work

		(NEB) enzyme. The PCR product and the vector pPD49.26 from Andy Fire's 1999 vector kit (Addgene) L754were digested with HindIII and PstI, purified and ligated.	
pNTC2	Vector for expressing proteins of interest in PVP neurons using the *dgn-1* promoter with ACPVN 3'UTR.	The ACPVN 3'UTR from pEXP294 was amplified using primers ATATCTGAGCTCatgaatcgttttaaaataacaaatc and ACGAAAGGGCCCgttaactcgaatcgctatccaag and NEB Phusion enzyme. The PCR fragment and pNTC1 were digested with SacI and ApaI before purification and ligation.	This work
pNTC3	*PVPp* promoter driving mCherry with *syn21* translational enhancer and ACPVN 3' UTR.	mCherry coding sequences were amplified using primers CCCTTGACCGGTaacttaaaaaaaaaaatcaaaATGGTCTCAAAGGGTGAAGAAG and ATTCATgaatgCCTTATACAATTCATCCATGCCAC via NEB Phusion. The 5' primer added the *syn21* translational	This work

		enhancer upstream of the translation start site. The PCR fragment and pNTC2 were digested with BmtI and SacI before purification and ligation.	
pNTC8	*PVPp* promoter driving GFP with *syn21* translational enhancer and ACPVN 3' UTR.	GFP coding sequences were amplified with CCCTTGGCTAGCaacttaaaaaaaaaaatcaaaatgagtaaaggagaagaactttcac and ATTCATGAGCTCtttgtatagttcatccatgccatg via NEB Phusion. The 5' primer added the *syn21* translational enhancer upstream of the translation start site. The PCR fragment and pNTC2 were digested with BmtI and SacI before purification and ligation.	This work
pNTC6	*PVPp* promoter driving HisCl1 with *syn21* translational enhancer and ACPVN 3' UTR.	Coding sequences for HisCl1 were amplified using promoters CCCTTGGCTAGCaacttaaaaaaaaaaatcaaaATGCAAAGCCCAACTAGC and ATTCATGAGCTCTCATAGGAACGTTGTCCAATAGA	This work

		C via NEB Phusion. The 5' primer added the *syn21* translational enhancer upstream of the translation start site. The PCR fragment and pNTC2 were digested with BmtI and SacI before purification and ligation.	
pNTC13	*ocr-3* promoter driving GFP with syn21 translational enhancer and ACPVN 3' UTR.	The *ocr-3* promoter was amplified from promoters TACGCCAAGCTTtttgggaatg aagttgtttagaaac and GTCGACCTGCAGgttgttagta agagtaaaatgaggaag via NEB Phusion. The 5' primer added the *syn21* translational enhancer upstream of the translation start site. The PCR fragment and pNTC8 were digested with HindII and PstI before purification and ligation.	This paper

Table 1-5: Cilia Markers Examined

Strain	**Marker**	**Reported Fluorescence**	**Notes**
BC10614	*bbs-8::GFP*	Associated with dendrites and cilia	Fluorescent puncta occasionally seen in PVP wing

CX3716	*osm-9::GFP*	Sensory	No fluorescence visible in PVP
GCX3695	*str-2::GFP*	Phasmid neurons	No fluorescence visible in PVP
GOU2162	*che-3::GFP*	most if not all sensory cilia	No fluorescence visible in late L4/adults in any neurons
GOU2187	*klp-20::GFP*	most if not all sensory cilia	No fluorescence visible in late L4/adults in any neurons
GOU2362	*ift-74p::GFP*	Most, if not all cilia	No fluorescence visible in late L4/adults in any neurons
LE310	*osm-6::GFP*	In winged amphid cilia	No fluorescence visible in PVP

Table 1-6: Supplementary References

Clark, S. G., Lu, X., & Horvitz, H. R. (1994). The Caenorhabditis elegans locus lin-15, a negative regulator of a tyrosine kinase signaling pathway, encodes two different proteins. *Genetics, 1*37(4), 987-997.

Lehrbach, N. J., Armisen, J., Lightfoot, H. L., Murfitt, K. J., Bugaut, A., Balasubramanian, S., & Miska, E. A. (2009). LIN-28 and the poly (U) polymerase PUP-2 regulate let-7 microRNA processing in Caenorhabditis elegans. *Nature structural & molecular biology*, 16(10), 1016-1020.

Martinez, N. J., Ow, M. C., Reece-Hoyes, J. S., Barrasa, M. I., Ambros, V. R., & Walhout, A. J. (2008). Genome-scale spatiotemporal analysis of Caenorhabditis elegans microRNA promoter activity. Genome research, 18(12), 2005-2015.

Maduro MF, & Pilgrim DB (1995). Identification and cloning of unc-119, a gene expressed in the Caenorhabditis elegans nervous system. *Genetics,* 141, 977-988.

Nguyen JP, Shipley FB, Linder AN, Plummer GS, Liu M, Setru SU, Shaevitz, JW, and Leifer AM (2016) Whole brain calcium imaging with cellular resolution in freely behaving Caenorhabditis elegans*. Proc Natl Acad Sci U S A* 113: E1074-1081.

Riddle, DL, Swanson MM, and Albert, PS (1981). Interacting genes in nematode dauer larva formation. Nature 290: 668-671.

Swoboda P, Adler HT, and Thomas JH (2000). The RFX-type transcription factor DAF-19 regulates sensory neuron cilium formation in C. elegans. Mol Cell 5: 411-421.

Results

The PVP neurons produce previously-uncharacterized branches at the midbody

While examining the *C. elegans* egg-laying system in a set of 20 strains in which the Green Fluorescent Protein (GFP) labels various sparse subsets of neurons (Fernandez et al. 2020), we noticed a neural structure that had not been previously described in the published literature. In two of the strains, a neural branch extended from the ventral nerve cord at the midbody near the vulva and terminated in a striking wing-shaped neural projection. Each of these two strains showed GFP labeling of its own set of ~20 types of neurons, with the overlap between these two sets being a pair of neurons with their cell bodies in the tail at positions consistent with those of the left and right PVP neurons. Using a transgene (*PVPp::GFP*) that drives GFP expression exclusively in PVP from a fragment of the dystroglycan promoter, we confirmed that the midbody neural branch structure was indeed produced by the PVP neurons (Figure 1-1A-B). The PVP neurons were previously classified based on reconstruction from electron micrograph (EM) serial sections as an interneuron pair with cell bodies located in the pre-anal ganglion that send processes anteriorly along the left and right ventral nerve cord (VNC) before terminating in the nerve ring located within the head of the animal (White et al. 1986). The midbody branches we observed, one produced by each PVP, extended dorsally from the VNC near the vulva and terminated over the uterus in a wing-like structure (Figure 1-1A.) The

branches were seen in hermaphrodites but not found in males (Figure 1-1B-C).

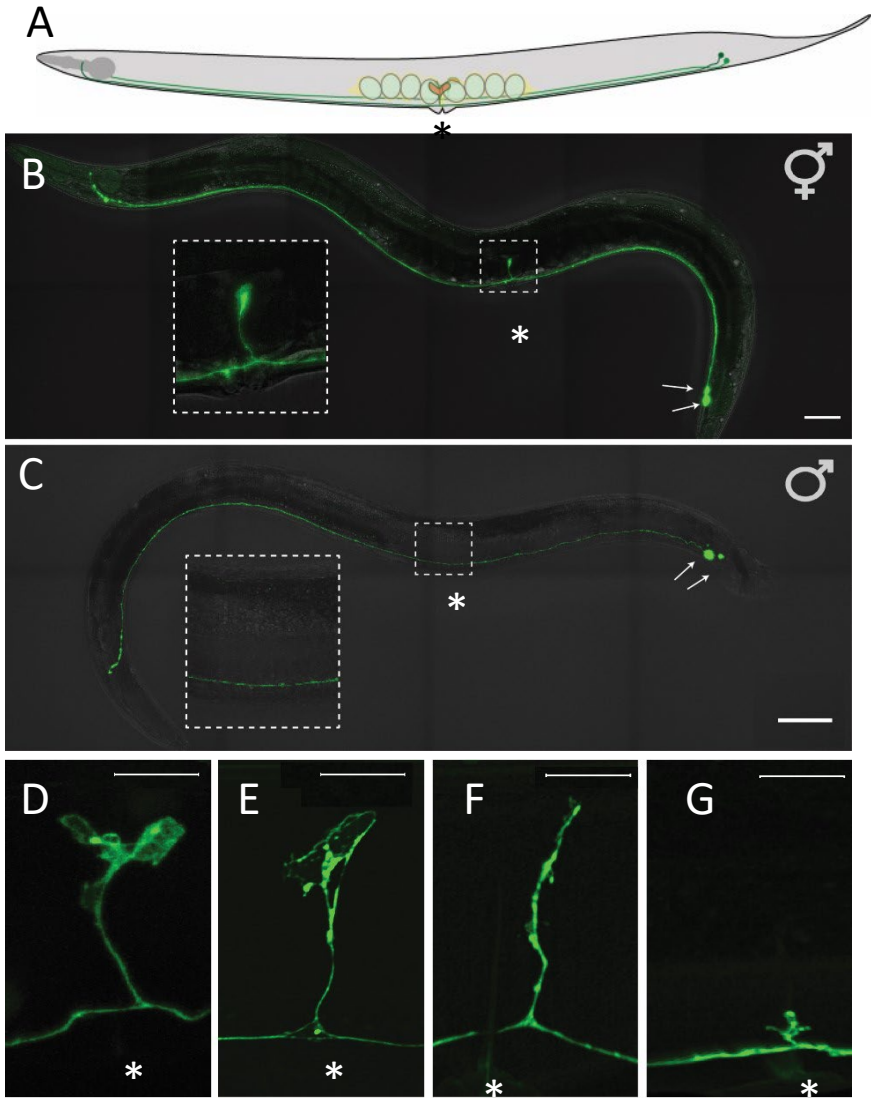

Figure 1-1: The PVP neuron pair produce a previously uncharacterized branch with wing-shaped endings at the midbody of adult hermaphrodite C. elegans.

(A) Diagram of PVP neurons within a *C. elegans* adult hermaphrodite. The left (light green) and right (dark green) PVPs have cell bodies near the tail (dots) and processes (lines) that cross as they go anteriorly along the ventral nerve cord to ultimately terminate in the head. Each PVP makes a branch near the vulva that terminates in a wing-like structure (red). In this and subsequent figures, an asterisk is placed just ventral to the vulval opening as a reference point. (B) PVP neurons visualized in an adult hermaphrodite carrying a transgene that expresses GFP from a PVP specific promoter (*PVPp*). Arrows indicate the PVP cell bodies. Inset magnifies the vulval region, where one PVP branch and wing are

visible in the focal plane shown. Scale bar, 50 μm. (C) Adult male with the male equivalents of the PVPs visualized as in (B). Inset magnifies the midbody region. The male neurons have no branch or wing. (D-G) Airyscan (super resolution) images of PVP in the vulval region demonstrating morphological variations in the branch and wing. Scale bars, 10 μm.

The PVP midbody branches were not described in the original EM reconstruction of the *C. elegans* nervous system (White et al. 1986), which caused us to be concerned that the GPF-labeled PVP branch we saw could be an artifact of the *PVPp::GFP* transgene. Significant deviations from the results of White et al. (1986) are almost unheard of, and these results have rather been confirmed by a vast body of subsequent work (e.g., Witlievet et al. 2021). Therefore, we obtained a set of three promoters that are expressed in PVP (among other cells) and used them to express GFP in transgenic animals. We noted that while the PVP branches generally ended in 'winged' shapes, we saw a wide variety of morphologies and lengths in different individual animals (Figure 1-1D-G).

PVP morphology and function are extremely sensitive to transgene expression

Originally, we intended to study the function of PVP and its branch by transgenically expressing a variety of proteins in PVP to record PVP activity (e.g., GCaMP) or manipulate PVP activity (e.g., channelrhodopsin, ChR2 or a histamine-gated chloride channel, HisCl), similar to studies our laboratory has carried out of other neurons of the egg-laying system (e.g., Collins et al. 2016). However, in the course of attempting to execute these experiments, it became evident that the PVPs are extremely sensitive to these transgenes. It was difficult to generate viable lines driving expression of any protein in PVP besides GFP: attempts to express channelrhodopsin and GCaMP resulted in animal death, whereas expression of red fluorescent proteins, such as mCherry and TagRFP, typically led to malformed PVP cells that often showed punctate red fluorescence, features that might indicate defects in PVP development or degeneration of the PVPs.

Of the transgenic strains mentioned above that we attempted to generate for functional assays of PVP, only one proved viable: a strain carrying a transgene that expressed both GFP and the HisCl channel from the PVP-specific promoter. This transgene was chromosomally integrated and outcrossed to the wild type to produce a clean genetic background, resulting in the "*PVPp::HisCl/PVPp::GFP*" strain. The GPF labeling of PVP in this strain is shown in Figure 1-1, and the PVP cells appear relatively healthy in this strain.

Transgenic worms expressing the HisCl channel can be treated with histamine to inactivate neurons that express the channel (Pokala et al. 2014). We assayed the *PVPp::HisCl/PVPp::GFP* animals for changes in behavior after treatment with histamine. We found that egg-laying behavior was relatively normal with or without histamine treatment, but that a locomotion behavior termed "roaming" (Flavell et al. 2013) appeared to be defective regardless of whether animals were treated with histamine or not (data not shown). Flavell et al. (2013) had previously shown that PVP neurons release the PDF-1 neuropeptide to promote roaming, and our results suggest that the *PVPp::HisCl/PVPp::GFP* transgene inactivated this function of PVP neurons even without the need activate the HisCl channels with histamine, as they phenocopied the *null* mutant of the PDF-1 receptor PDFR-1. Thus, we conclude that likely all of our transgenes that are expressed in PVP, even those that show the most healthy-appearing PVP morphology, compromise the function of PVP.

The sensitivity of PVP function to transgenes raised the question of whether the morphologies of the branch and wing structures of PVP were also affected by transgenes used to visualize them. We re-examined other transgenic lines with GPF expression in PVP, *dop-6::GFP* and *odr-2p::GFP* to confirm that the winged branches themselves were not merely an artefact (Figure 1-2).

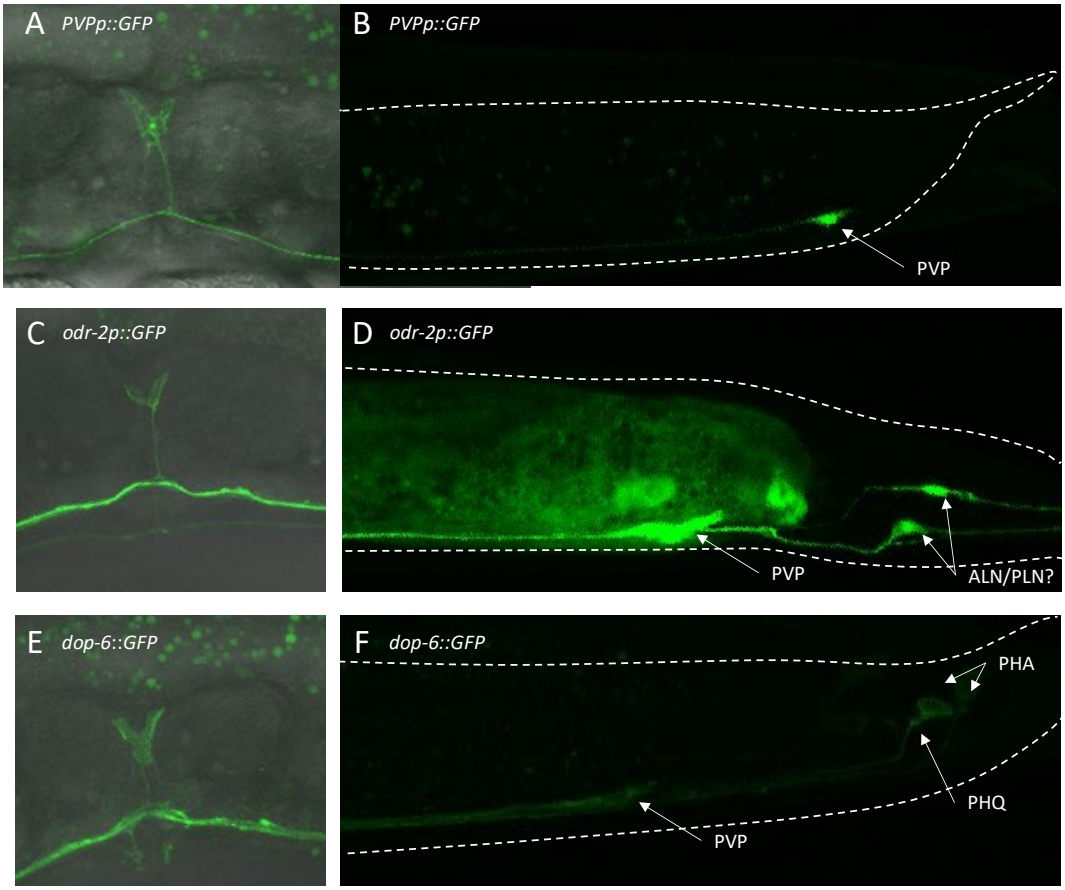

Figure 1-2: Confirmation of PVP cells produce wing-shaped structures with different GFP reporters

Comparing the *PVPp::GFP* (A-B) marker to lines known to have PVP-expression, *odr-2p* (C-D) and *dop-6* (E-F), the identity of the PVP cells as the neurons that produce the winged structures at the midbody were confirmed. *n = 20* per line. This also confirmed that the winged structures themselves were not an artefact.

Interestingly, while we originally observed the PVP wing-structure extending dorsally from the VNC at the midbody (Figures 1-1, Figure 1-2), we also sometimes observed PVP wing-structures curved ventrally towards the vulva (Figure 1-3B). This occurred a little less than 50% of the time in *PVPp::HisCl/PVPp::GFP* animals (9 out of 20 animals examined; Figure 1-2C). While the wing structure was always present along with the PVP cell body and main VNC process in *PVPp::HisCl/PVPp::GFP* (and *PVP::GFP*) animals, conversely in the *odr-2p::GFP* animals, we observed dorsally-oriented PVP wing structures 54% (*n*=8) of the time,

ventral orientations 26% (*n*=4), and no visible branches for the remaining 20% (*n*=3*)* (total *n*=15). We also expressed GFP under a the *ocr-3b* promoter, which like our original *dgn-1*-derived promoter, is specific to PVP in adult animals (Lorenzo et al. 2020). These *ocr-3p::GFP* animals had fluorescent PVP neurons in which no branch or wing structure was visible (*n*=15), and on three occasions, the main ventral cord process of the PVP neurons terminated at a point between the vulva and the head and failed to reach its normal more anterior destination in the nerve ring of the head (Figure 1-3F). All this together suggests the PVP branch and wing structures are sensitive to transgene expression, and that the variations in branch and wing in animals that carry the same *PVPp::HisCl/PVPp::GFP* transgene (Figures 1-1D-F) may be due to effects of the transgene itself. That being the case, the most common PVP morphology seen, and the one reproduced in multiple independent transgenic lines, is that with a dorsal branch terminating in a large wing-like structure, as seen in Figures 1-1D-G. This most likely represents the morphology of a healthy PVP.

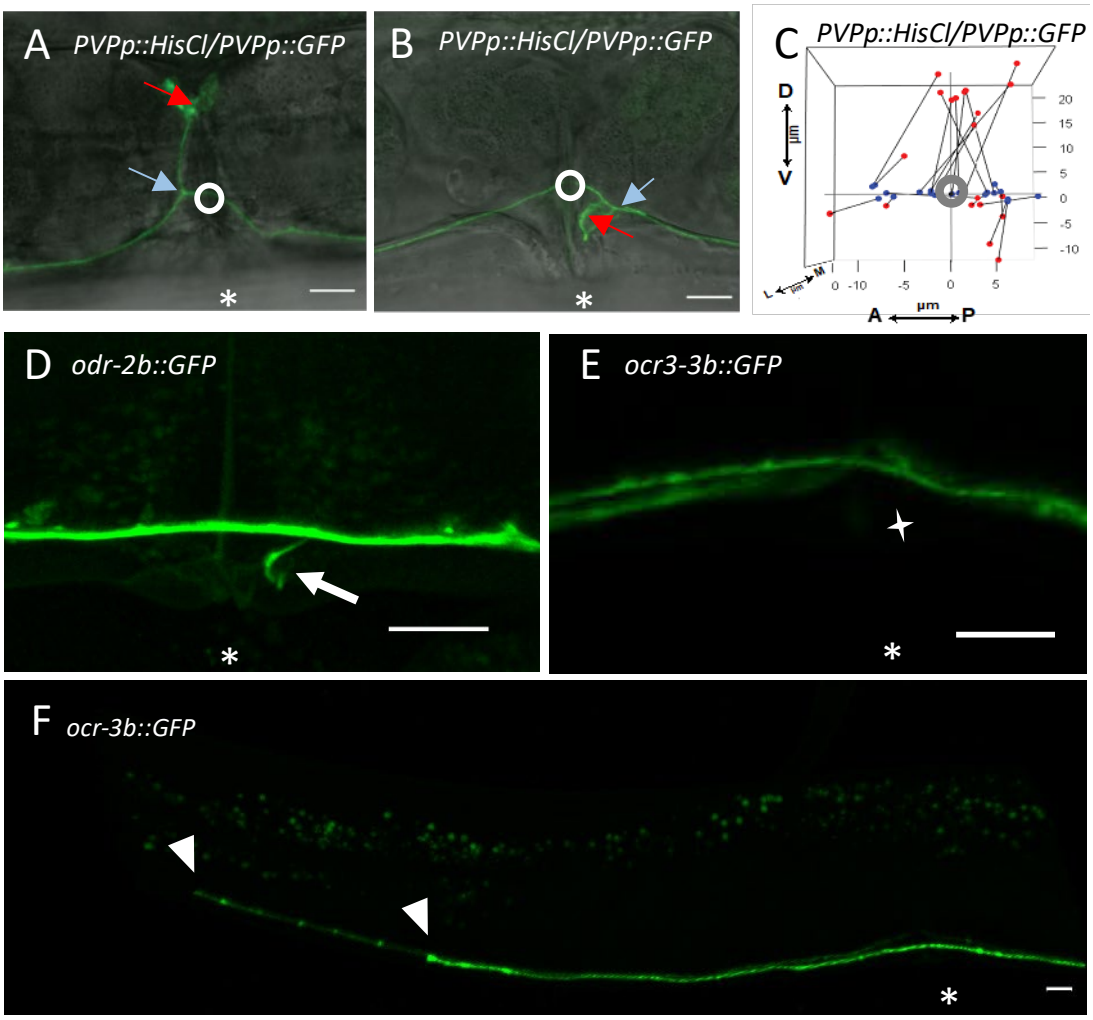

Figure 1-3: PVP neurons are sensitive to transgene expression

Representative confocal images of a dorsally-extending PVP branch/wing structure (A) and a ventrally-oriented PVP branch/wing structure (B) in *PVPp::HisCl/PVPp::GFP* animals. Grey circles enclose the points where main PVP process crosses the vulval slit, blue arrows indicate the PVP branch point, and red arrows indicating the approximate center of the PVP wing structure. (C) Graph showing the 3Dimensional positions of the branch points (blue dots) and wing centers (red dots) for 20 PVP neurons in *PVPp::HisCl/PVPp::GFP* animals (in which PVP wing structures always accompany PVPs), with these two reference points for each PVP neuron connected by a black line. Axes of the graph are the dorsal/ventral, anterior/posterior, and lateral/medial axes of the animal, and the origin of the graph (grey circle) is the point at which the main PVP process crosses the vulval slit. (D-F) PVPs expressing GFP display morphological variations that can depend on the promoter (indicated on each panel) used to express GFP. (D) A ventrally-directed PVP branch (arrow); (E) PVP main processes pass the vulval region without making branches; (F) PVP main processes with no branch at the vulval region that terminate (arrowheads) before reaching their normal destinations in the head. Scale bars, 10 μm in all panels.

The PVP branch and wing develops at the L4 stage and lie within the egg-laying system

Because the PVP branch and wing lies near the egg-laying system of adult hermaphrodites, we asked if this structure develops at the L4 larval stage, when the cells of the egg-laying system differentiate (Desai et al. 1988). We imaged animals throughout the L4 larval stage (Figure 1-4), visualizing PVP with the *PVPp::HisCl/PVPp::GFP* transgene, and visualizing the outlines of vulval and uterine cells that form the main structural elements of the egg-laying system with an *ajm-1::mCherry* transgene that labels the apical junctions of these cells (Köppen et al. 2001). We staged the animals according to vulval morphology as early, mid, or late L4 (Mok et al 2015). Early L4 animals showed no PVP branches (n=10), about 40% of the animals had some sort of branch in mid L4 (n=10), and all animals in the late L4 stage showed branches (n=10).

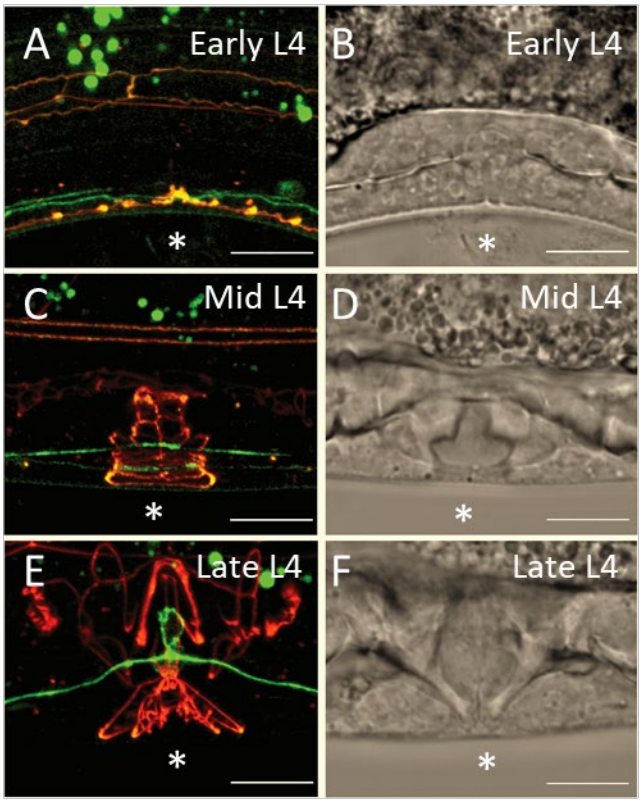

Figure 1-4: The PVP develop within the L4 larval stage.

Region of the developing vulva in L4 animals carrying the *PVPp::GFP* transgene to visualize PVP neurons and the *ajm-1::mCh* transgene to label the apical junctions of epithelial cells, imaged by confocal fluorescence. Left panels show fluorescence images that reveal the developing morphology of the PVP (green) and the developing morphology of structural cells of the vulva and uterus (red). Right panels show brightfield images of the same animals, in which morphology of the developing vulva is also seen. (A-D) In early L4 and mid L4 animals the PVP passes by the vulva without consistently showing branches. (E-F) Late L4 animals have consistently initiated PVP branching. Scale bars, 10μm.

We examined the anatomical relationship of the PVP branch and wing to cells of the egg-laying system in adult animals using GFP to mark PVP and mCherry to mark specific cells of the egg-laying system. As noted previously, some variations in PVP morphology may be artifacts of the transgenes used to visualize PVP, so the most constant features of PVP anatomy are likely the most meaningful. The point at which the branch leaves the main ventral cord process may be either just anterior or just posterior to the vulval opening, ranging over a ~15 μm span relative to the vulva (Figure 1-3). Despite this variation, the wing structure in which the branch terminates is consistently located at the junction between the vulva and the uterus. Figure 1-5A schematizes the structural cells of the adult egg-laying system whose apical junctions are labeled by the *ajm-1::mCh* transgene. Unlaid eggs are stored in the uterus, which is a tube constructed from a set of uterine toroid (ut) cells and a uterine seam cell. Eggs are laid by passing through connection between the uterus and vulva formed by the dorsal uterine (du) cell and the uterine-vulval (uv) cells. Finally, the eggs proceed out of the animal through a tube formed by the vulval toroid (vt) cells. Despite variations in origin and path of the PVP branch, in *PVPp::HisCl1/PVPp::GFP; ajm-1::mCh* adult animals, when PVP branches proceed dorsally they consistently (10/10 animals examined) terminate in wings that lie over junction of the uv and du cells (Figure 1-5B).

Figure 1-4C shows a diagram of the neurons of the egg-laying system that are labeled by an *ida-1::mCh* transgene. The uv1s are neuroendocrine cells that form part of the uterine-vulval connection. As shown in Figure 1-4D, in *PVPp::HisCl1/PVPp::GFP; ida-1::mCh* adult animals, PVP wing structures consistently lie just dorsal to the uv1s and between the anterior

and posterior uv1 cells (10/10 animals examined). This again places the uv1 wings directly over the uterine-vulval connection. On occasion we have observed smaller tendrils or branches extending off of the main wing structure extending towards the HSN and uv1 neurons, close to the large synaptic junctions made by the HSN.

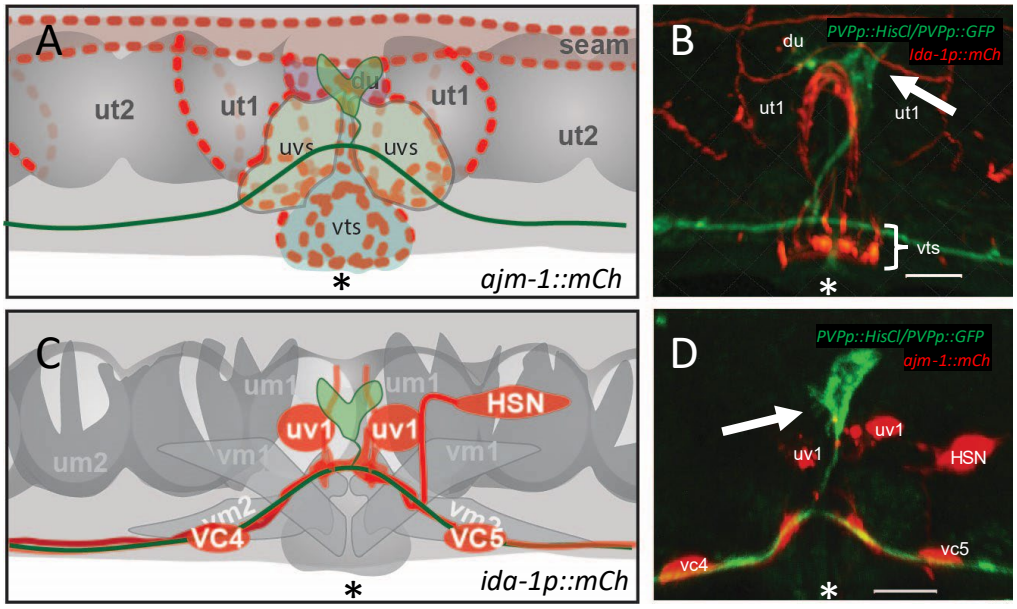

Figure 1-5: PVP wing and branches lie at the connection between the vulva and the uterus of the egg-laying system.

(A-B) Schematic (A) and confocal image (B) of on the left side of the egg-laying system of an animal expressing *PVPp::GFP* (green) and *ajm-1::mCh* (red). Cells outlined by the *ajm-1::mCh* marker include the uterine toroid cells (ut1 and ut2), vulval toroid cells (vts), dorsal uterine cell (du), and uterine seam cell (seam). The PVP wing (arrow in B) consistently lies over the du cell. (C-D) Schematic (C) and confocal image (D) of the left side of the egg-laying system of an animal expressing *PVPp::GFP* (green) and *ida-1p::mCh* (red). Schematic indicates muscle cells and neurons of the egg-laying system, including the uterine muscles cells (um1 and um2), vulval muscle cells (vm1 and vm2), uv1 neuroendocrine cells, and VC and HSN neurons. Neural cells are labeled with *ida-1p::mCh*. PVP wings (arrow) are centrally located between and dorsal to the uv1s. Scale bars, 10 µm.

The PVP wing structures show some but not all features of sensory cilia

The anatomy of the PVP branch and wing are reminiscent of the anatomy of dendrites and ciliated endings of sensory neurons in *C. elegans*. In particular, the PVP wing appears similar

to the wing-like ciliated ending AWC amphid neuron of the head. We wondered if the PVP wing structures could be cilia as well. We injected both the *PVPp::GFP* transgene and an *odr-1p::RFP* transgene, which labels the AWC and AWB sensory neurons, into a genetic background (*daf-19; daf-12*) that disrupts the structures of sensory cilia (Senti and Swoboda 2008). The *daf-19* mutation disrupts cilia, while the *daf-12* mutation is necessary to suppress otherwise lethal effects of the *daf-19* mutation. Thus, the *daf-12* single-mutant background is used as a control in this experiment. Extrachromosomal, mosaic animals were mounted and examined under a confocal microscope (see methods) to first assess if the animal expressed both GFP in at least one PVP (approx. 1 out of 6 animals) and RFP in at least one amphid cilium for comparison within individuals (approximately 1 out of 4 animals). In the *daf-12* control background, the AWC and PVP wing-like endings appeared similar and were present in both cell types in all animals examined (Figures 1-6A and 1-6D). In the *daf-19; daf-12* "cillialess" background, wing-like cilia were absent from almost 60% of AWC neurons examined, although the sensory dendrites were still present (Figure 1-6B and 1-6C). However, in these same *daf-19; daf-12* animals, the wing structure was still present in 12/14 of PVP neurons examined (Figures 1-6E and 1-6F).

We examined a variety of *C. elegans* strains available that were reported to mark neural sensory cilia in young larval stages with fluorescent proteins, but these strains either did not show visible fluorescence in PVP or did not visibly express the fluorescent reporter protein in any neurons at the L4 or adult stages.. This line of experimentation thus failed to provide any further support for the hypothesis that the PVP wings are sensory cilia.

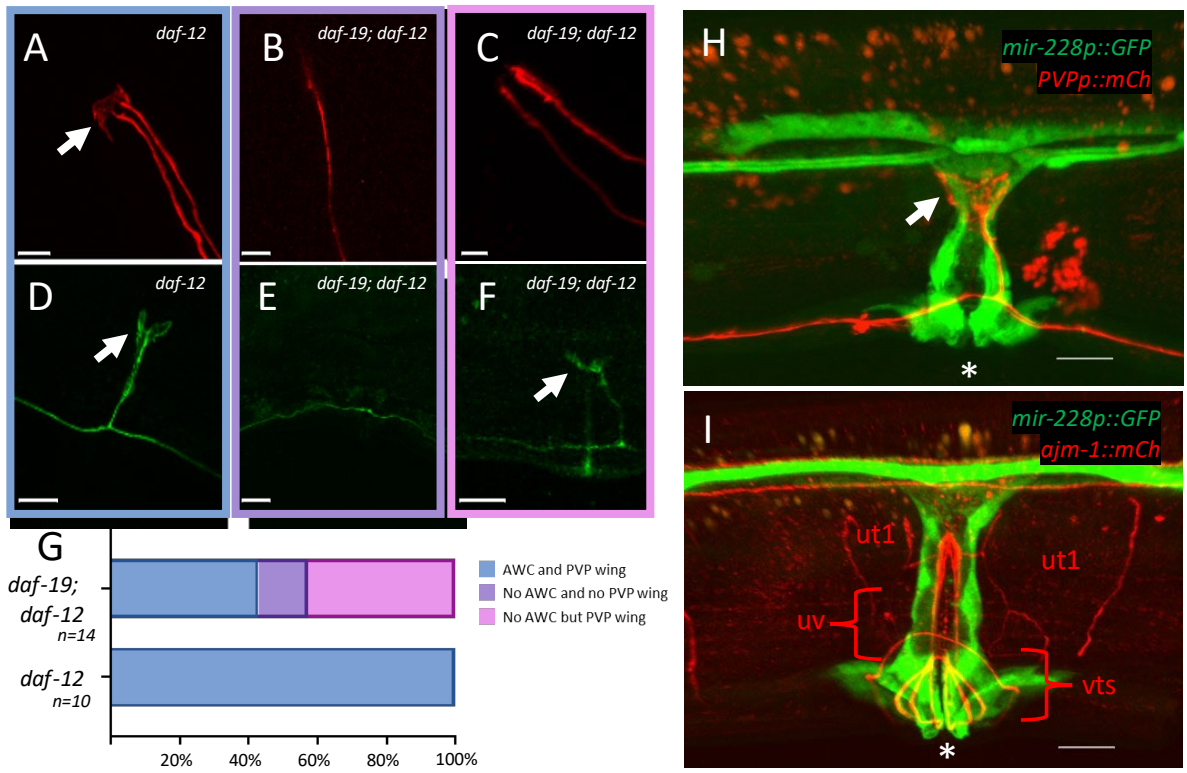

Figure 1-6: PVP branches and wing lie among cells that express a glial marker, but are only rarely affected by a mutation that disrupts sensory cilia.

(A-F) The *PVPp::GFP* transgene that labels the PVP (green) and an *odr-1p::RFP* transgene that labels the AWC and AWB ciliated sensory neurons (red) were both crossed into the *daf-12* mutant background (A, D), in which cilia are normal, and into the *daf-19; daf-12* double-mutant background (B, C, E, F), in which sensory cilia are disrupted. In *daf-12* animals, the AWC sensory dendrites terminate in winged cilia (A, arrow), and the PVP branch terminates in a similar-appearing winged structure (D, arrow). In the *daf-19; daf-12* double-mutant, almost 8/14 animals lack amphid winged cilia (B, C). In this same background, PVP branches and wings were missing in only 2/14 animals examined (E), and the remaining animals (*n*=12) showed PVP branches and wings (F, arrow indicates wing). (G) Quantification. (H) The PVP branch and wing (red) lie within cells labeled by the mir-*228p::GFP* glial marker (green). Scale bar, 10 µm. (I) The a*jm-1::mCh* marker (red) serves as a reference to help identify the cells expressing *mir-228p::GFP* (green). Scale bar, 10 µm.

Sensory dendrites and cilia in *C. elegans* are surrounded by glial cells (Shaham 2006), and we tested whether the PVP dendrite and wing share this feature. We crossed a *PVPp*::*mCh* transgene that labels PVP with red fluorescence into a strain carrying a transgene (*mir-228p::GFP*) that labels all glial cells with green fluorescence (Fung et al. 2020; Pierce et al.

2008). In the resulting double-labeled strain, we saw that the PVP branch and wing were surrounded by cells that expressed the glial marker (Figure 1-5H). Previously, it has been noted that the *mir-228p::GFP* marker labels cells near the vulva (Pierce et al. 2008, Fung et al. 2020), but these cells were not identified and had not been considered to be candidates to be *bona fide* glial cells since no neural sensory endings at the vulva were known. We crossed the *mir-228p::GFP* transgene to the *ajm-1::mCh* transgene that outlines structural cells of the egg-laying system (Figure 1-5I). While a definitive identification of the midbody cells that express the *mir-228* glial marker will require a more detailed analysis, it appears that they include vulval toroid (vt) cells, one or more of the uterine-vulval (uv) cell types, as well as additional uterine cells. Regardless of the exact identity of these cells, the fact that the PVP branch and wing are surrounded by cells that express the *mir-228* glial marker supports the hypothesis that the PVP branch is a sensory dendrite and the PVP wing is a sensory cilium.

Discussion

The goal of this work was to investigate previously uncharacterized neural branches near the *C. elegans* egg-laying system. The neurons that generate egg-laying behavior constitute an intensively-studied model neural circuit, so the discovery of a new component of this circuit could enhance the power of this model system to provide insights into how neural circuits in general function. It has been a great rarity to discover new features of any C. *elegans* neuron since the ground-breaking study of White et al. (1986) provided a virtually complete description of the anatomy and connectivity of all neurons in the hermaphrodite worm. We speculate that this absence of the PVP wing structures were missed because of a) the small *n*-number in the original traces and b) the dorsal/ventral positioning that is more likely to get lost in the vertical slices required by EM that traced through the animal in a predominately anterior to posterior orientation. However, it first was observed in 1999 that the PVP neurons made previously undescribed branches near the hermaphrodite vulva (O. Hobert and D. Hall, personal communication). We determined that neural branches we observed near the hermaphrodite vulva indeed arise from the PVP neurons, and we present here our initial characterization of the structure of the PVP branches and their possible functions.

We found that the PVP neurons have hermaphrodite-specific branches whose development and structure suggest they function in some aspect of reproduction. The PVP neurons were previously described as being born near the tail during embryonic development and then extending processes to the head, with the right PVP (PVPR) process crossing the ventral midline to serve as a pioneer for the left tract of the ventral nerve cord (Durbin, 1987; Wadsworth and Hedgecock, 1996; Wadsworth et al. 1996). The PVPs were also previously known to be sexually dimorphic, since the cells that differentiate as PVPL and PVPR in hermaphrodites instead become the PVU and PVS neurons in males, respectively (White et al. 1986; Cook et al. 2019). We found that in hermaphrodite PVP neurons—but not in males

PVU and PVS neurons—the main neural processes sprout branches at the midbody that typically extend dorsally and terminate in large wing-like structures that lie over the connection between the uterus and vulva. This is the connection through which hermaphrodites receive sperm into the uterus when they are mated by males, and through which eggs pass out of the uterus when they are laid. The PVP branches are hermaphrodite-specific since they are not seen in the male PVU or PVS neurons. Further, the PVP branches develop at a time during the L4 stage when other sexually dimorphic structures of the hermaphrodite also develop, such as the vulva and the neurons of the egg-laying circuit (Desai et al. 1988; Mok et al. 2015). These observations are all consistent with the hypothesis that the PVP neurons carry out functions related to adult hermaphrodite reproduction, such as mating or egg laying.

Are the PVP neurons ciliated sensory neurons?

The PVP branches terminate in structures that could be sensory cilia, although the evidence for this remains equivocal. The wing-like termini of the PVP branches are about 10 μm across, and the most similar neural structures in the *C. elegans* nervous system are the "winged" cilia of the AWC amphid neurons, which occur at the termini of AWC dendrites near the nose of the animal. AWC neurons use these winged cilia primarily to respond to volatile odorants (Bargmann et al. 1993). Thus, we hypothesized that the PVP branch termini might also be sensory cilia. In favor of this hypothesis are three lines of evidence. First, the PVP branch endings morphologically resemble AWC cilia. Second, we found that the PVP branches and wings are surrounded by cells that express the *mir-228p::GFP* marker, which is commonly used as a glial-specific marker in *C. elegans*, and dendrites and cilia of known sensory neurons are similarly surrounded by glial cells that express this same marker (Shaham 2006). Third, the PVP neurons were found by Vidal et al. (2018) to express the sensory receptor homologs *srab-12* and *sri-9*. Interestingly, *sri-9* appears to be expressed in only dauer animals

and then only in the left but not right PVP. This asymmetry between PVPL and PVPR is reminiscent of the asymmetries between the left and right members of *C. elegans* sensory neuron pairs such as ASE (Yu et al. 1997), PLM (Wicks and Rankin 1995), and AWC (Troemel et al. 1999), the latter of which are the sensory neurons with cilia similar in shape to the PVP wing structures.

Standing against the three lines of evidence that favor the hypothesis that PVP are ciliated sensory neurons are two types of experiments that gave negative results. First, the *daf-19* mutation, which disrupts the structure of cilia in known sensory neurons (Swoboda et al. 2000), had a far less striking effect on PVP. While ~60% of the winged cilia of AWC neurons were disrupted in the *daf-19* mutant background, only ~7% of PVP branches and wings were affected in the *daf-19* background. Second, we were unable to see GFP labeling of the PVP winged endings using transgenes that label sensory cilia in young larvae, although we were also not able to detect labeling of any of these sensory cilia with these transgenes in adult hermaphrodites, the only types of animals that have PVP branches and wings.

We conclude that it is a reasonable hypothesis that the PVP branches and wings are sensory dendrites and cilia, and that the surrounding structural cells of the egg-laying system may play a secondary role as glial cells that support these PVP structures. However, given that these would be quite surprising results to come up only now after decades of previous studies of the *C. elegans* egg-laying system, further experimental evidence is needed before a final conclusion can be reached about this issue.

Challenges to studying PVP function

While we note that more experimental evidence about PVP function is required to make firm conclusions about its function, this article lacks such evidence because of technical challenges specific to the study of PVP. We tried multiple different promoters to express

multiple different proteins in PVP, including fluorescent proteins, and we repeatedly found that these transgenes either failed to produce viable transgenic animals (perhaps due to disrupting the ventral cord pioneer function of PVPR), or resulted in viable transgenic lines in which PVP neurons had variable and "sick" appearing morphology. Our efforts exclusively used multicopy transgenes, and perhaps single-copy transgenes or CRISPR engineering of endogenous genes will be more successful.

What are plausible functions for PVP?

We did not detect any defects in egg-laying behavior in our transgenic animals carrying transgenes designed to inactivate PVP, but we did detect locomotion defects (data not shown). PVP is known to release the neuropeptide PDF-1 to promote long bouts of forward locomotion known as roaming, which contrast to an alternate pattern of locomotion in which animals make more reversals and stay in place, known as dwelling (Flavell et al. 2013). If PVP is a sensory neuron with a cilium, then it could sense mechanical or chemical signals from the hermaphrodite reproductive system over which the winged cilium lies. Therefore, PVP could sense something about mating or egg laying to regulate PDF-1 release and the switch between roaming and dwelling locomotion.

If PVP is a sensory neuron, one possibility is that it mechanically senses either eggs in the uterus, or the passage of eggs out of the uterus when eggs are laid. The accumulation of eggs in the uterus is sensed by a mechanism that remains unidentified (Collins et al. 2016), and the PVP could play a role in this mechanism. Egg-laying and locomotion behavior are coordinated by mechanisms that also remain undiscovered (Collins and Koelle, 2013), and again PVP could play a role in this process. Alternatively, as sensory neurons, PVPs could allow hermaphrodites to sense when they are being mated by males. For instance, the PVP wing structure could mechanically sense physical distortion from mating and contribute to regulating responses such evading males and/or expelling sperm (Kleemann and Basolo

2007). Since PVPs express chemoreceptors, it could also be the case that the PVP wing structures participate in pheromone signaling as part of the interplay between aging and mating (Ludewig et al. 2019; Aprison and Ruvinsky 2016; Maures et al. 2014). While these ideas remain hypothetical, they can direct further studies aimed at uncovering PVP function.

Acknowledgements

We thank Dr. Richard Ikegami for supplying us with pEXP294, which contained the PVP-specific promoter referred to in this manuscript as PVPp. We also thank the CGC for supplying strains and Wormbase for the plethora of genetic information.

Literature Cited

Albertson, D.G., and J. Thompson, 1976 The pharynx of Caenorhabditis elegans. Philosophical Transactions of the Royal Society of London. B, Biological Sciences 275 (938):299-325.

Aprison, E.Z., and I. Ruvinsky, 2016 Sexually antagonistic male signals manipulate germline and soma of C. elegans hermaphrodites. Current Biology 26 (20):2827-2833.

Banerjee, N., R. Bhattacharya, M. Gorczyca, K.M. Collins, and M.M. Francis, 2017 Local neuropeptide signaling modulates serotonergic transmission to shape the temporal organization of C. elegans egg-laying behavior. PLoS genetics 13 (4):e1006697.

Bargmann, C.I., Hartwieg, E., and H.R. Horvitz, 1993 Odorant-selective genes and neurons mediate olfaction in C. elegans. Cell 74(3):515-527.

Bargmann, C.I., and E. Marder, 2013 From the connectome to brain function. Nature methods 10 (6):483-490.

Barrios, A., R. Ghosh, C. Fang, S.W. Emmons, and M.M. Barr, 2012 1 neuropeptide signaling modulates a neural circuit for mate-searching behavior in C. elegans. Nature neuroscience 15 (12):1675-1682.

Boothe, T., L. Hilbert, M. Heide, L. Berninger, W.B. Huttner et al., 2017 A tunable refractive index matching medium for live imaging cells, tissues and model organisms. Elife 6:e27240.

Brenner, S., 1974 The genetics of Caenorhabditis elegans. Genetics 77 (1):71-94.

Collins, K.M., A. Bode, R.W. Fernandez, J.E. Tanis, J.C. Brewer et al., 2016 Activity of the C. elegans egg-laying behavior circuit is controlled by competing activation and feedback inhibition. Elife 5:e21126.

Cook, S.J., T.A. Jarrell, C.A. Brittin, Y. Wang, A.E. Bloniarz et al., 2019 Whole-animal connectomes of both Caenorhabditis elegans sexes. Nature 571 (7763):63-71.

Desai, C., Garriga, G., McIntire, S.L., and H.R. Horvitz, 1988 A genetic pathway for development of the Caenorhabditis elegans HSN motor neurons. Nature 336(6200):638-646.

Duerr, J.S., J. Gaskin, and J.B. Rand, 2001 Identified neurons in C. elegans coexpress vesicular transporters for acetylcholine and monoamines. American Journal of Physiology-Cell Physiology 280 (6):C1616-C1622.

Duerr, J.S., H.P. Han, S.D. Fields, and J.B. Rand, 2008 Identification of major classes of cholinergic neurons in the nematode Caenorhabditis elegans. Journal of Comparative Neurology 506 (3):398-408.

Evans, T.C., 2006 Transformation and microinjection. WormBook 10.

Fay, D.S., 2013 Classical genetic methods. WormBook: the online review of C. elegans biology:1.

Fernandez, R.W., K. Wei, E.Y. Wang, D. Mikalauskaite, A. Olson et al., 2020 Cellular expression and functional roles of all 26 neurotransmitter GPCRs in the C. elegans egg-laying circuit. Journal of Neuroscience 40 (39):7475-7488.

Flavell, S.W., N. Pokala, E.Z. Macosko, D.R. Albrecht, J. Larsch et al., 2013 Serotonin and the neuropeptide PDF initiate and extend opposing behavioral states in C. elegans. Cell 154 (5):1023-1035.

Fung, W., L. Wexler, and M.G. Heiman, 2020 Cell-type-specific promoters for C. elegans glia. Journal of neurogenetics 34 (3-4):335-346.

Gendrel, M., E.G. Atlas, and O. Hobert, 2016 A cellular and regulatory map of the GABAergic nervous system of C. elegans. Elife 5:e17686.

Hardaker, L.A., E. Singer, R. Kerr, G. Zhou, and W.R. Schafer, 2001 Serotonin modulates locomotory behavior and coordinates egg-laying and movement in Caenorhabditis elegans. Journal of neurobiology 49 (4):303-313.

Kessler, R.C., W.T. Chiu, O. Demler, and E.E. Walters, 2005 Prevalence, severity, and comorbidity of 12-month DSM-IV disorders in the National Comorbidity Survey Replication. Archives of general psychiatry 62 (6):617-627.

Kleemann, G.A., and A.L. Basolo, 2007 Facultative decrease in mating resistance in hermaphroditic Caenorhabditis elegans with self-sperm depletion. Animal Behaviour 74 (5):1339-1347.

Koelle, M.R., 2018 Neurotransmitter signaling through heterotrimeric G proteins: insights from studies in C. elegans. WormBook: The Online Review of C. elegans Biology [Internet].

Lorenzo, R., M. Onizuka, M. Defrance, and P. Laurent, 2020 Combining single-cell RNA-sequencing with a molecular atlas unveils new markers for Caenorhabditis elegans neuron classes. Nucleic acids research 48 (13):7119-7134.

Ludewig, A.H., A.B. Artyukhin, E.Z. Aprison, P.R. Rodrigues, D.C. Pulido et al., 2019 An excreted small molecule promotes C. elegans reproductive development and aging. Nature chemical biology 15 (8):838-845.

Maures, T.J., L.N. Booth, B.A. Benayoun, Y. Izrayelit, F.C. Schroeder et al., 2014 Males shorten the life span of C. elegans hermaphrodites via secreted compounds. Science 343 (6170):541-544.

Mok, D.Z., P.W. Sternberg, and T. Inoue, 2015 Morphologically defined sub-stages of C. elegans vulval development in the fourth larval stage. BMC developmental biology 15 (1):1-8.

Nguyen, J.P., F.B. Shipley, A.N. Linder, G.S. Plummer, M. Liu et al., 2016 Whole-brain calcium imaging with cellular resolution in freely behaving Caenorhabditis elegans. Proceedings of the National Academy of Sciences 113 (8):E1074-E1081.

Pereira, L., P. Kratsios, E. Serrano-Saiz, H. Sheftel, A.E. Mayo et al., 2015 A cellular and regulatory map of the cholinergic nervous system of C. elegans. Elife 4.

Pfeiffer, B.D., J.W. Truman, and G.M. Rubin, 2012 Using translational enhancers to increase transgene expression in Drosophila. Proceedings of the National Academy of Sciences 109 (17):6626-6631.

Pierce, M.L., M.D. Weston, B. Fritzsch, H.W. Gabel, G. Ruvkun et al., 2008 MicroRNA-183 family conservation and ciliated neurosensory organ expression. Evolution & development 10 (1):106-113.

Senti, G., and P. Swoboda, 2008 Distinct isoforms of the RFX transcription factor DAF-19 regulate ciliogenesis and maintenance of synaptic activity. Molecular biology of the cell 19 (12):5517-5528.

Serrano-Saiz, E., R.J. Poole, T. Felton, F. Zhang, E.D. De La Cruz et al., 2013 Modular control of glutamatergic neuronal identity in C. elegans by distinct homeodomain proteins. Cell 155 (3):659-673.

Shaham, S., 2006. Glia–neuron interactions in the nervous system of Caenorhabditis elegans. Current opinion in neurobiology, 16(5):522-528.

Shyn, S.I., R. Kerr, and W.R. Schafer, 2003 Serotonin and Go modulate functional states of neurons and muscles controlling C. elegans egg-laying behavior. Current Biology 13 (21):1910-1915.

Swoboda, P., Adler, H.T. and J.H. Thomas, 2000 The RFX-type transcription factor DAF-19 regulates sensory neuron cilium formation in C. elegans. Molecular cell, 5(3):411-421.

Troemel, E.R., A. Sagasti, and C.I. Bargmann, 1999 Lateral signaling mediated by axon contact and calcium entry regulates asymmetric odorant receptor expression in C. elegans. Cell 99 (4):387-398.

Tursun, B., L. Cochella, I. Carrera, and O. Hobert, 2009 A toolkit and robust pipeline for the generation of fosmid-based reporter genes in C. elegans. PLoS One 4 (3):e4625.

Vidal, B., U. Aghayeva, H. Sun, C. Wang, L. Glenwinkel et al., 2018 An atlas of Caenorhabditis elegans chemoreceptor expression. PLoS biology 16 (1):e2004218.

Waggoner, L.E., G.T. Zhou, R.W. Schafer, and W.R. Schafer, 1998 Control of alternative behavioral states by serotonin in Caenorhabditis elegans. Neuron 21 (1):203-214.

White, J.G., E. Southgate, J.N. Thomson, and S. Brenner, 1986 The structure of the nervous system of the nematode Caenorhabditis elegans. Philos Trans R Soc Lond B Biol Sci 314 (1165):1-340.

Wicks, S.R., and C.H. Rankin, 1995 Integration of mechanosensory stimuli in Caenorhabditis elegans. Journal of Neuroscience 15 (3):2434-2444.

Xu, M., T.A. Jarrell, Y. Wang, S.J. Cook, D.H. Hall et al., 2013 Computer assisted assembly of connectomes from electron micrographs: application to Caenorhabditis elegans. PLoS One 8 (1):e54050.

Yu, S., L. Avery, E. Baude, and D.L. Garbers, 1997 Guanylyl cyclase expression in specific sensory neurons: a new family of chemosensory receptors. Proceedings of the National Academy of Sciences 94 (7):3384-3387.

A. Appendix 1: Additional Comments on PVP

Additional commentary and notes on the information described in the paper from the previous chapter.

Results

As mentioned in the previous chapter, having procured a PVP-specific promoter, I originally planned to use a well-established battery of cell-specific assays to determine the function of the PVPs. I cloned the *PVPp* promoter from Richard Ikegami's Gateway vector and placed it within the pPD49.26 Andy Fire vector, where I designed a cloning procedure to drop in genes of interest at MSCII (see methods in Chapter 1). I cloned in a histamine-gated chloride channel (HisCl1; Pokala et al. 2014), channelrhodopsin (ChR2; Nagel et al. 2005), and GCaMP5. HisCl and ChR2 were intended to allow me to turn the cell on and off and then observe any consequent behavioral of functional changes; conversely, GCaMP5 was to allow me to observe when the cell is active as the animal moves freely (Collins et al. 2016).

The extra-chromosomal lines made with the *PVPp* promoter using *lin-15* as an injection marker made expression difficult to ascertain: in the *PVPp* animals, only 1 out of 6 animals expressed GFP in the PVP, and only 1 out of 20 animals expressed GFP in both (data not shown). Furthermore, the PVP nuclei are small, and coupled with faint expression even after boosting expression with the *syn21* enhancer and AcPVN 3'UTR (Pfeiffer et al. 2012), the cells were difficult to see under a dissecting microscope, preventing screening for potential lines. Furthermore, each of the constructs resulted in their own issues: firstly, *PVPp::ChR2* was not visible at any injection concentration (despite multiple injection mix compositions and attempts) which made it impossible to select lines for work with this system. Secondly, *PVPp::GCaMP5* was not also visible in any lines. At this point, I was concerned that there was a general problem with my injecting technique, so to test this, I performed an experiment

where I created a *PVPp::mCh* line, and injected various ratios of *PVPp::mCh*, *PVPp::GCaMP5*, or both to determine if *PVPp::GCaMP5* was toxic. As shown in Table A-4, any time any amount of *PVPp::GCaMP5* is injected, there are no viable lines, which suggests that the *PVPp::GCaMP5* construct was making the animal or the cell sick to the point that transgene expression could not be seen. While it may not be surprising to see toxicity particularly at the higher concentrations, these concentrations followed established injection concentrations and have not caused this level of toxicity when driven by other promoters (Collins et al. 2016).

Table A-1: Injection mix ratios and progeny counts of PVPp::GCaMP5 and PVPp::mCherry Injections

Injection Trial		**A**	**B**	**C**	**D**	**E**	**F**
Ratio of Injection Mix	*PVPp::GcAMP* (µg/µL)	50	0	0	25	80	100
	PVPp::mCh (µg/µL)	0	50	20	20	20	20
# of Animals After Injection	# of P0s injected	14	10	12	12	10	10
	# of F1 singled	45	~100	~100	~100	~100	~30
	# of F2 non-muv Lines	5	11	9	10	7	2
	# of F3 Stable "non-muv lines"	0	5	5	0	0	0

Thirdly, the HisCl construct initially was created with an SL2 promoter, which concerned me that this might compromise the expression of the protein. I therefore removed the SL2 promoter and co-expressed *PVPp::GFP* and *PVPp::HisCl*. This *did* result in viable, GFP-expressing lines which were then integrated by standard methods (Fernandez et al. 2020), but it also presented the problem of not knowing if the *PVPp::HisCl* was expressing properly. This was exacerbated by the fact that preliminary behavioral assays utilizing *PVPp::HisCl* did not show a change in egg-laying: neither early-stage egg-laying assays where strains are assayed for hyperactivity of the egg-laying circuit, nor unlaid egg-laying assays where strains are assayed for disruptions in the egg-laying circuit demonstrated any significant difference (Figure A-1). Of course, this negative data does not necessarily mean that the HisCl channel was not expressing properly; rather, it could have meant that the PVPs were not participating in this function.

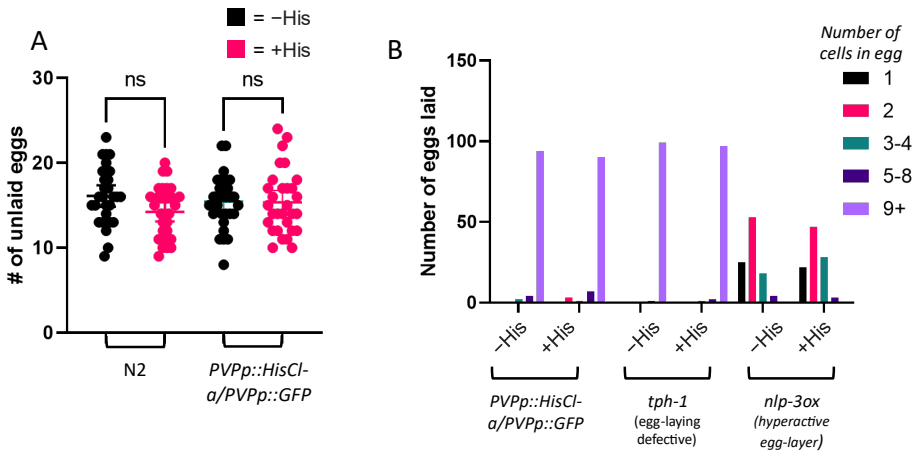

Figure A-1: Unlaid egg and early-stage egg laying assays of PVPp::HisCl/PVPp::GFP.

(A) Unlaid egg assay on *PVPp::HisCl/PVPp::GFP* animals demonstrates that PVP does not have an effect on egg-retention. 30 animals were assayed 30 hours post L4 by dissolving the hermaphrodites in bleach and counting the eggs. (B) Early-stage egg laying assay on *PVPp::HisCl/PVPp::GFP* animals demonstrates that PVP does not have an effect on rate of egg-laying. 30 animals laid eggs for 30 minutes 30-hours post L4 and 100 eggs were scored for the number of cells, with less than 8 being early, and compared to a *tph-1* egg-laying defective mutant and an *nlp-3ox* hyperactive egg-layer.

Because of PVP's predicted role in locomotion, I performed a locomotion assay on *PVPp::HisCl/PVPp::GFP* animals and compared that to the *pdf-1* animals. PDF-1 is a key neuropeptide that encourages roaming in the roaming/dwelling circuit and is expressed in the PVPs. Therefore, if the *PVPp::HisCl/PVPp::GFP* line were working as expected, the histamine-treated animals should somewhat recapitulate *pdf-1* animals: that is, in an assay where animals are left to explore a plate and their exploration is scored by aligning the plate with a grid in which squares are counted, the *PVPp:HisCl/PVPp::GFP* animals treated with histamine should be similar to the *pdf-1* mutants and explore less squares than the control. This was not the case; instead, in typical conditions, *PVPp::HisCl/PVPp::GFP* phenocopies *pdf-1,* which suggests that rather than making an inducible construct that would hyperpolarize PVP, the construct was instead constitutively damaging or inactivating the cell (Figure A-2).

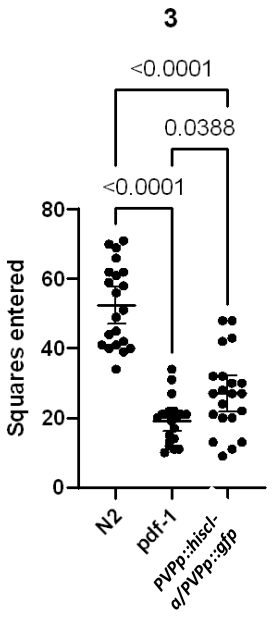

Figure A-2: Motility test of PVPp::HisCl/PVPp::GFP.

This test demonstrates that PVP has an effect on locomotion, and that the *PVPp::HisCl/PVPp::GFP* line is constitutively affecting the animal, rather than inducible. Animals were singled out on a freshly seeded

NGM plate and left to roam on the plate for 3 hours. The plate was placed on a grid, and the tracks were scored. The *PVPp::HisCl/PVPp::GFP* line, not on histamine phenocopied the *pdfr-1* mutant. PVP is known to express *pdf-1*, meaning that the PVPs are not functioning properly in the *PVPp::HisCl/PVPp::GFP* line.

Simple red fluorescent protein promoters, such as such as mCherry and TagRFP, caused the cell to become much filled with puncta, more so than what I observed in GFP expressing animals (Figure A-3); these strains also occasionally expressed fluorescent protein in other cells in the head that was not observed in GFP expressing strains (Figure A-4). Concerned that this was somehow caused by the transition from the Gateway vector to the pPD49.26 Fire vector, I expressed GFP using the Fire vector as well, and saw no abnormalities compared with the Gateway vector (Figure A-5). This suggests it was not the backbone plasmid that was toxic to the PVPs, but rather the PVP cells are sensitive to transgene expression under this promoter. This is not entirely uncommon in *C. elegans*; for example, the HSN promoter (Dong et al. 2000) and the VC promoter (Bany et al. 2003) both cause the respective neurons to degrade.

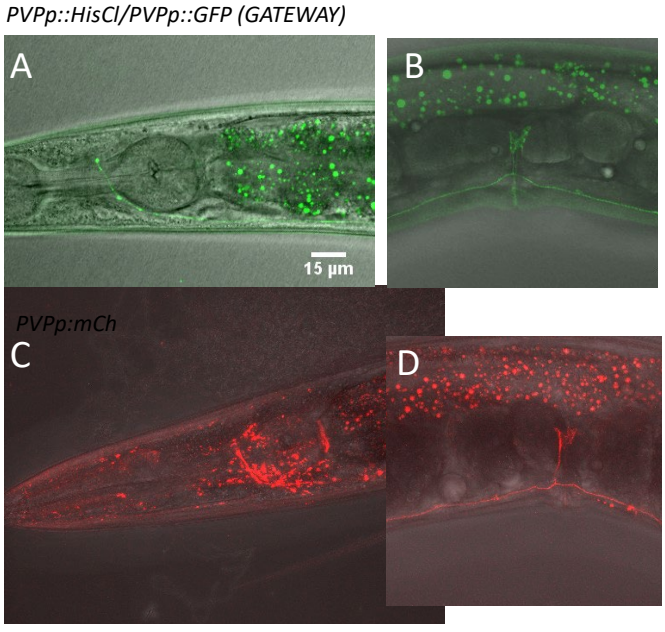

Figure A-3: The PVPp promoter is sensitive to even red fluorescent marker mCherry.

(A) Head and (B) midbody of *PVPp::GFP* in Gateway plasmid and (C) *PVPp::mCherry* head and (D) midbody in pPD49.26 Fire Vector. In (C&D) the wing and VNC is much more punctate, and there is large increase in puncta in the nerve ring which is not present in the GFP expressing animals.

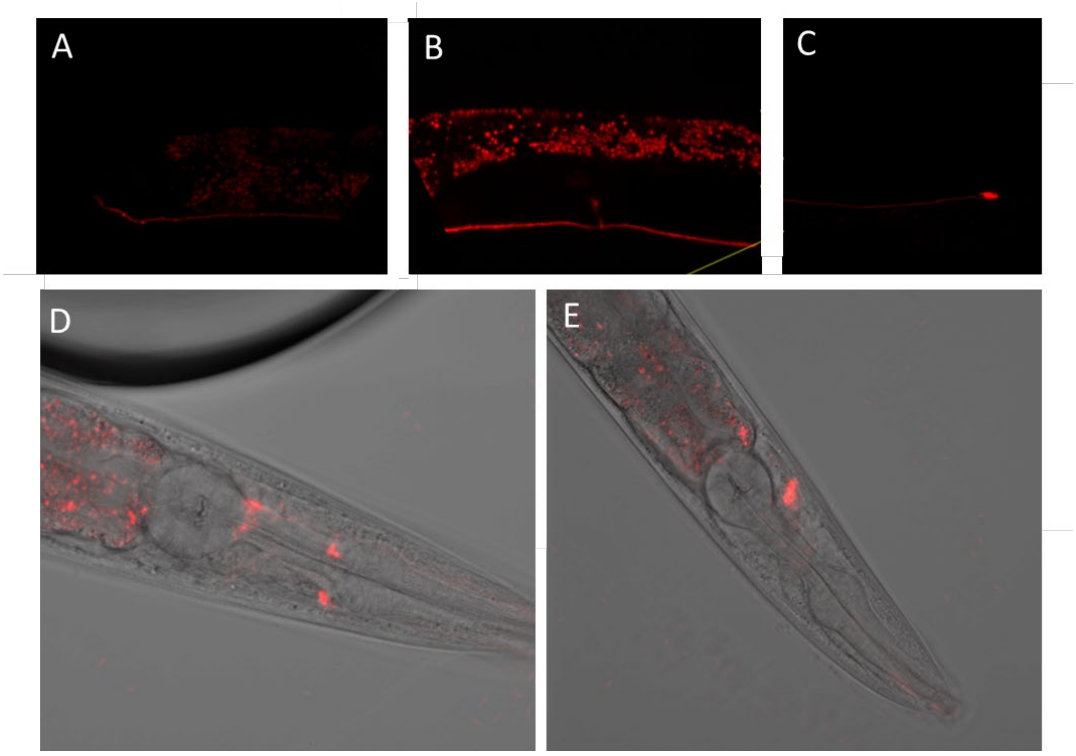

Figure A-4: The sensitivity to red proteins is not limited at mCherry.

Top: *PVPp::TagRFP* in the head (A), midbody (B) and tail (C) with less puncta and more cell specificity than mCherry. Bottom: (D-E) Two separate adult *PVPp::TagRFP* hermaphrodites expressing TagRFP in unidentified head neurons.

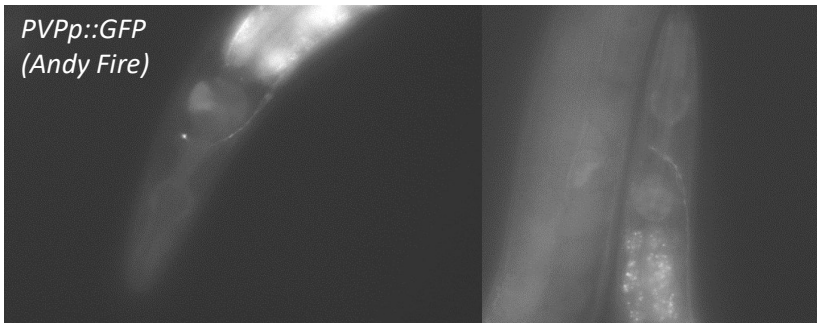

Figure A-5: PVPp::GFP (pPD49.26 backbone) is specific to PVP with no toxicity.

PVPp::GFP in the pPD49.26 Fire vector confirms that the toxicity from the *PVPp* transgenes is not due to the Fire backbone, as expression in the head is consistently specific to PVP alone.

To attempt to remedy this, I also expressed GFP under a different PVP-specific promoter, *ocr-3* (Lorenzo et al. 2020). This was an additional attempt to solve the issues surrounding the PVP promoter—I hoped that a different promoter would fix the expression change and toxicity. Unfortunately, while GFP expression under the *ocr-3* promoter was highly specific to the PVP and far less mosaic than *PVPp* (as opposed to 1/6 animals expressing GFP in PVP in the PVPp line, the *ocr3p::GFP* line expressed GFP in PVP in 1/3 animals), there was no instance in which a branch or wing structure was visible (n=15), and on at least one occasion, the main process of the PVP neurons did not reach the nerve cord.

That the PVP wing structures are positioned differently along the dorsal-ventral axis in percentages that change depending on the transgene driving GFP expression (see Chapter 1) suggests that this observation is an artefact of transgene sensitivity, rather than a legitimate feature of the structure. This evidence together concludes that the PVP wing structures are sensitive to transgene expression, regardless of the promoter driving that expression.

Discussion

Despite lacking a functional output for the PVP cells, I reasoned that the *PVPp::HisCl* at minimum morphologically matched the other fluorescent markers, and therefore could be

utilized to gain some understanding of this previously undescribed cell structure. This resulted in the paper from the previous chapter, in which the main findings were as follows:

1) The wing structures branch off at the PVP at the midbody of *C. elegans* (Figure 1-1)
2) The branches are hermaphrodite-specific and not found in males (Figure 1-1)
3) The structure develops in the mid-L4 stage and persists throughout adulthood (Figure 1-3)
4) While the structures are generally 'winged' shaped, there is a wide variety of morphologies and lengths from individuals (Figure 1-1G-J).
5) The PVP wing structures develop at the junction between the vulval toroid cells and dorsal uterine cell (Figure 1-4). At this position, the PVPs are also in close proximity to both the hermaphrodite-specific cells (HSNs) and the neuroendocrine uv1 cells.
6) PVP wing structures show some, but not all features, of sensory cilia. The PVP wing structures resemble amphid wing cilia; are surrounded by cells expressing the *mir-228p::GFP* marker, which is often used as a pan-glial marker; and three others have reported that it expresses sensory receptor homologs. Even so, the PVP wing structures do not behave as the AWB/AWC winged cilia did in "cilialess" mutants and I was unable to detect labeling of the PVP wing using transgenes that label sensory cilia in young larvae. (Figure 1-5)

As stated in the previous section, currently the known function of the PVP neurons is almost exclusively tied to locomotion. The PVPs are sexually dimorphic neurons; in males they are PVU and PVS and in hermaphrodites are PVPL and PVPR (White et al. 1986; Cook et al. 2019). The PVPs are cholinergic (Duerr et al. 2008), and both the hermaphroditic and male cells express the neuropeptide PDF-1 (Barrios et al. 2012). In males, PDF-1 has been shown to drive male exploration in mate searching (Barrios et al. 2012) and in hermaphrodites PDF-1 has shown to drive roaming behavior (Flavell et al. 2013; Barrios et al. 2012),

characterized by increased forward speed and fewer reversals. Roaming behavior is juxtaposed by dwelling, which is controlled by the release of serotonin by the NSM neuron, located in the head of the animal.

Interestingly, the egg-laying circuit is also activated by the release of serotonin via the HSNs (Waggoner et al. 1998; Shyn et al. 2003)—of which the PVP wing structure is in close proximity—and facilitated by acetylcholine released by the VC4/VC5 motor cord neurons (Duerr et al. 2001; Collins et al. 2016). While there have been several observations that tie locomotion to egg laying, none have been mechanistically explained. For example, it has been observed that animals tend to increase forward speed before egg laying and reverse after (Hardaker et al. 2001). Given the PVPs' known neurotransmitters and their relationship with locomotion, I hypothesize that the PVPs are linking locomotion to egg laying. This could be true regardless of the correct morphological definition of the structures, be that they are cilia, large synapses, or other varicosities. For example, if the PVPs were ciliated, they could be sensing the physical distortion of the uterine lumen in a similar way that the uv1 neuroendocrine cells (Banerjee et al. 2017) and signal for some locomotion behavior. If they were to be other structures that would still function in this way, they could be large synapses that join with the large synaptic cleft where the HSN, VC4-5 motor cord neurons, and uv1 neuroendocrine cells communicate and effect vulval muscle activity.

Alternatively, given their position and development, the PVP wing structures could link mating to locomotion: for instance, the structure could be sensing physical distortion from mating and contribute to regulating responses such evading males and/or expelling sperm (Kleemann and Basolo 2007). Knowing that the PVPs are reported to express chemoreceptors, it could also be the case that these wing structures are participating in pheromone signaling that could be at the interplay between aging and mating (Ludewig et al. 2019; Aprison and Ruvinsky 2016; Maures et al. 2014). The predicted chemoreceptor SRI9 is only expressed in

PVPL after exiting dauer diapause (Vidal et al. 2018), further suggesting a role in development. This asymmetry between PVPL and PVPR is reminiscent of the asymmetries of sensory neurons such as ASE (Yu et al. 1997), PLM (Wicks and Rankin 1995), and AWC (Troemel et al. 1999), the latter of which possessing winged cilia similar in shape to the PVP wing structures.

My findings here in which I demonstrate that the PVP neurons develop large, sexually-dimorphic winged structures at the midbody of adult hermaphrodites should better inform the *C. elegans* community who wish to fill in the blanks of current model neural circuits.

Additional Materials and Methods

N.B. Other methods are previously described in Chapter 1. The assays described below are based off of standard assays (Chase and Koelle 2004).

Brood Assay

L4 animals were staged and cloned out onto either standard NGM plates or NGM plates + 10mM histamine. Each animal was singled out onto a new plate every 24 hours for 4 days. Broods were counted 3 days later, when the brood reached the L4 larval stage. n=5. The data were then statistically analyzed using a student t-test for statistical difference from the control. 95% confidence interval is displayed.

Mating Assay

Similar to the brood assay, L4 animals were staged and cloned out onto either standard NGM plates or NGM plates + 10mM histamine. Each hermaphrodite was paired with 3 males that expressed *myo-2::mCh,* a bright mCherry marker labeling the pharynx muscles. The hermaphrodite and the males were transferred to a new plate every 24 hours, and progeny were counted 3 days later, with those expressing the mCherry marker scored as cross-progeny. n=5, except for 72-96 hours due to animal death over time. The data were then statistically

analyzed using a student *t*-test for statistical difference from the control. 95% confidence interval is displayed.

Early-stage egg-laying assay

Animals were staged at the L4 stage. 29 hours later, 30 animals were transferred to either freshly seeded NGM plate or NGM + 10mM histamine to acclimate for 30 minutes. Then, animals were transferred to another fresh plate of the same type. Plates were placed at 20°C for exactly 30 minutes, at which point the eggs were staged under a Lieca Wildfield M420 microscope. Eggs were visually staged according to how many cells they had, with <8 being considered 'early' and all other egg types being termed 'late.' The data were then statistically analyzed using a student *t*-test for statistical difference from the control. 95% confidence interval is displayed.

Unlaid egg assay

Animals were staged at the L4 stage. At 29.5 hours post L4, 30 animals were transferred to either freshly seeded NGM plate or NGM + 10mM histamine to acclimate for 30 minutes. Then, at 30 hours post L4, individual animals were placed in a 7µL drop of 20% commercial bleach on the lid of a 96-well tissue culture dish. After approximately 10 minutes, the adult animals dissolved, but the bleach-resistant fertilized eggs could be seen and counted under a dissecting microscope. n=30. The data were then statistically analyzed using a student *t*-test for statistical difference from the control. 95% confidence interval is displayed.

Motility Test

Animals were staged at the L4 stage. At 29.5 hours, animals were placed on a freshly seeded NGM plate. The individual animals were cloned out to on a fresh plate and left to roam for 3 hours. A grid was then placed under the plate and the number of squares the trail left behind by the animals crawling was scored (Flavell et al. 2013). The data were then statistically

analyzed using a student *t*-test for statistical difference from the control. 95% confidence interval is displayed.

Strains, Plasmids, and Transgenes

N.B. Lines also used in Chapter 1 are not listed here, but can be found in the Methods section of Chapter 1.

Table A-2: Supplemental strains used in Appendix 1

Strain	**Genotype**	**Features**	**Source**
LX2620	*lin-15(n765ts) X; vsIs279*	Carries a chromosomally integrated transgene with that includes plasmids pNTC6 (*PVPp::HisCl)*, pL15EK (rescues the l*in-15* phenotype), and pEXP294 (*PVPp::GFP).* This was viewed to have weaker GFP expression than LX2622, which was used in the main paper of this work.	This study
MT15434	*tph-1(mg280) II*	*tph-1* knockout used as a control for egg-laying defective animals.	Sze et al, 2000
LX1978	*lin-15(n765ts) X ; vsEx748*	*nlp-3* overexpressing used as a positive control for hyperactive egg laying in the early-stage egg laying assay.	Brewer et. al, 2019
CX14295	*pdfr-1(ok3425) III*	A positive control animal that has decreased locomotion on food.	Flavell et al., 2013

Table A-3: Supplement alleles used in this study

Allele	**Relevant features**	**For transgenes constructed in this study: injection components**	**Source**
lin-15(n765ts) X	Temperature-sensitive multi-vulva phenotype. Used in strains that are recipients for transgene injections since it is rescued by the pL15EK plasmid, carrying a wild-type copy of *lin-15.*	N/A	Clark et al., 1994
tph-1(mg280) II	*tph-1* knockout. Used to study locomotion and egg laying defects.	N/A	Sze 2000 et al., 2000
vsIs279	Integrated *PVPp::HisCl/PVPp::GFP*. Animals were treated with UV/TMP and screened for integration.	pNTC6 (*pDGN1::HisCl*) at 50ng/µL, pExP294 (*pDGN1::GFP*) at 50ng/µL, pL15EK at 50ng/µL, digested *E. coli* DH5a genomic DNA at 25ng/µL	This study
vsEx748	Transgenic rescue of *lin-15* multi-vulval phenotype. Hyperactive egg laying phenotype, as observed by	N/A	Brewer et. al, 2019

	unlaid egg assay and stage of freshly laid eggs assay.		
pdfr-1(ok3425) III	Null deletion of PDFR-1 receptor. Dwelling increases from wild type levels.	N/A	Flavell et al. 2013

Table A-4: Plasmids used in this study

Plasmid Name	**Features**	**Construction**	**Source**
pL15EK	Contains a wild-type copy of the *lin-15* gene. Used as a co-injection marker to rescue the *lin-15* phenotype.		Clark et al., 1994
pEXP294	Expression of GFP specifically in PVP neurons. A fragment of the *dgn-1* promoter driving GFP with *syn21* translational enhancer and ACPVN 3' UTR.	Gateway cloning	A gift from Richard Ikegami

pNTC5	*PVPp* promoter driving Channelrhodopsin (ChR2) with *syn21* translational enhancer and ACPVN 3' UTR.	GFP coding sequences were amplified with CCCTTGGCTAGCaacttaaaaaaaaa aatcaaaATGGATTATGGAGGC GCCC and GAGCTCTTACTTGTACAGCTC GTCCATGCCGAGAGTGATCC C via NEB Phusion. The 5' primer added the *syn21* translational enhancer upstream of the translation start site. The PCR fragment and pNTC2 were digested with BmtI and SacI before purification and ligation.	This work
pNTC12	*PVPp* promoter driving GCaMP5 with *syn21* translational enhancer and ACPVN 3' UTR.	GFP coding sequences were amplified with CCCTTGGCTAGCaacttaaaaaaaaa aatcaaagatctcgccaccatgggttctcatcatc and ATTCATGAGCTCgctcacttcgctgtc atcatttgtacaaactcttcgtagtttacc via NEB Phusion. The 5' primer added the *syn21* translational enhancer upstream of the translation start site. The PCR fragment and pNTC2 were	This work

		digested with BmtI and SacI before purification and ligation.	
pNTC11	*PVPp* promoter driving TagRFP with *syn21* translational enhancer and ACPVN 3' UTR.	GFP coding sequences were amplified with CCCTTGGCTAGCaacttaaaaaaaaa aatcaaaATGGTGTCTAAGGGCG AAGAGCTGATTAAGG and ATTCATGAGCTCTCAATTAAG TTTGTGCCCCAGTTTGC via NEB Phusion. The 5' primer added the *syn21* translational enhancer upstream of the translation start site. The PCR fragment and pNTC2 were digested with BmtI and SacI before purification and ligation.	This work

Literature Cited

Aprison, E.Z., and I. Ruvinsky, 2016 Sexually antagonistic male signals manipulate germline and soma of C. elegans hermaphrodites. Current Biology 26 (20):2827-2833.

Banerjee, N., R. Bhattacharya, M. Gorczyca, K.M. Collins, and M.M. Francis, 2017 Local neuropeptide signaling modulates serotonergic transmission to shape the temporal organization of C. elegans egg-laying behavior. PLoS genetics 13 (4):e1006697.

Bany, I.A., M.-Q. Dong, and M.R. Koelle, 2003 Genetic and cellular basis for acetylcholine inhibition of Caenorhabditis elegans egg-laying behavior. Journal of Neuroscience 23 (22):8060-8069.

Barrios, A., R. Ghosh, C. Fang, S.W. Emmons, and M.M. Barr, 2012 1 neuropeptide signaling modulates a neural circuit for mate-searching behavior in C. elegans. Nature neuroscience 15 (12):1675-1682.

Chase, D.L., and M.R. Koelle, 2004 Genetic analysis of RGS protein function in Caenorhabditis elegans. Methods in enzymology 389:305-320.

Collins, K.M., A. Bode, R.W. Fernandez, J.E. Tanis, J.C. Brewer et al., 2016 Activity of the C. elegans egg-laying behavior circuit is controlled by competing activation and feedback inhibition. Elife 5:e21126.

Cook, S.J., T.A. Jarrell, C.A. Brittin, Y. Wang, A.E. Bloniarz et al., 2019 Whole-animal connectomes of both Caenorhabditis elegans sexes. Nature 571 (7763):63-71.

Dong, M.-Q., D. Chase, G.A. Patikoglou, and M.R. Koelle, 2000 Multiple RGS proteins alter neural G protein signaling to allow C. elegans to rapidly change behavior when fed. Genes & development 14 (16):2003-2014.

Duerr, J.S., J. Gaskin, and J.B. Rand, 2001 Identified neurons in C. elegans coexpress vesicular transporters for acetylcholine and monoamines. American Journal of Physiology-Cell Physiology 280 (6):C1616-C1622.

Duerr, J.S., H.P. Han, S.D. Fields, and J.B. Rand, 2008 Identification of major classes of cholinergic neurons in the nematode Caenorhabditis elegans. Journal of Comparative Neurology 506 (3):398-408.

Fernandez, R.W., K. Wei, E.Y. Wang, D. Mikalauskaite, A. Olson et al., 2020 Cellular expression and functional roles of all 26 neurotransmitter GPCRs in the C. elegans egg-laying circuit. Journal of Neuroscience 40 (39):7475-7488.

Flavell, S.W., N. Pokala, E.Z. Macosko, D.R. Albrecht, J. Larsch et al., 2013 Serotonin and the neuropeptide PDF initiate and extend opposing behavioral states in C. elegans. Cell 154 (5):1023-1035.

Hardaker, L.A., E. Singer, R. Kerr, G. Zhou, and W.R. Schafer, 2001 Serotonin modulates locomotory behavior and coordinates egg-laying and movement in Caenorhabditis elegans. Journal of neurobiology 49 (4):303-313.

Kleemann, G.A., and A.L. Basolo, 2007 Facultative decrease in mating resistance in hermaphroditic Caenorhabditis elegans with self-sperm depletion. Animal Behaviour 74 (5):1339-1347.

Lorenzo, R., M. Onizuka, M. Defrance, and P. Laurent, 2020 Combining single-cell RNA-sequencing with a molecular atlas unveils new markers for Caenorhabditis elegans neuron classes. Nucleic acids research 48 (13):7119-7134.

Ludewig, A.H., A.B. Artyukhin, E.Z. Aprison, P.R. Rodrigues, D.C. Pulido et al., 2019 An excreted small molecule promotes C. elegans reproductive development and aging. Nature chemical biology 15 (8):838-845.

Maures, T.J., L.N. Booth, B.A. Benayoun, Y. Izrayelit, F.C. Schroeder et al., 2014 Males shorten the life span of C. elegans hermaphrodites via secreted compounds. Science 343 (6170):541-544.

Nagel, G., M. Brauner, J.F. Liewald, N. Adeishvili, E. Bamberg et al., 2005 Light activation of channelrhodopsin-2 in excitable cells of Caenorhabditis elegans triggers rapid behavioral responses. Current Biology 15 (24):2279-2284.

Pfeiffer, B.D., J.W. Truman, and G.M. Rubin, 2012 Using translational enhancers to increase transgene expression in Drosophila. Proceedings of the National Academy of Sciences 109 (17):6626-6631.

Pokala, N., Q. Liu, A. Gordus, and C.I. Bargmann, 2014 Inducible and titratable silencing of Caenorhabditis elegans neurons in vivo with histamine-gated chloride channels. Proceedings of the National Academy of Sciences 111 (7):2770-2775.

Shyn, S.I., R. Kerr, and W.R. Schafer, 2003 Serotonin and Go modulate functional states of neurons and muscles controlling C. elegans egg-laying behavior. Current Biology 13 (21):1910-1915.

Troemel, E.R., A. Sagasti, and C.I. Bargmann, 1999 Lateral signaling mediated by axon contact and calcium entry regulates asymmetric odorant receptor expression in C. elegans. Cell 99 (4):387-398.

Vidal, B., U. Aghayeva, H. Sun, C. Wang, L. Glenwinkel et al., 2018 An atlas of Caenorhabditis elegans chemoreceptor expression. PLoS biology 16 (1):e2004218.

Waggoner, L.E., G.T. Zhou, R.W. Schafer, and W.R. Schafer, 1998 Control of alternative behavioral states by serotonin in Caenorhabditis elegans. Neuron 21 (1):203-214.

White, J.G., E. Southgate, J.N. Thomson, and S. Brenner, 1986 The structure of the nervous system of the nematode Caenorhabditis elegans. Philos Trans R Soc Lond B Biol Sci 314 (1165):1-340.

Wicks, S.R., and C.H. Rankin, 1995 Integration of mechanosensory stimuli in Caenorhabditis elegans. Journal of Neuroscience 15 (3):2434-2444.

Yu, S., L. Avery, E. Baude, and D.L. Garbers, 1997 Guanylyl cyclase expression in specific sensory neurons: a new family of chemosensory receptors. Proceedings of the National Academy of Sciences 94 (7):3384-3387.

B. Appendix 2: NeuroPAL

The work described in this appendix contributed to the publication entitled "Using NeuroPAL Multicolor Fluorescence Labeling to Identify Neurons in *C. elegans*" which was submitted to *Current Protocols* on 19 June 2022 of which I am 2nd author.

Introduction

The model system of the *C. elegans* nervous system contains a small number of neurons that have been the focus of exploratory research endeavors, including: 1) the physical connectome detailing all the synaptic connections between these neurons (White et al. 1986); 2) the neurotransmitter map detailing which neurotransmitters are released by which neurons (Gendrel et al. 2016); and most recently 3) the transcriptome detailed at the single-cell level (Taylor et al. 2021) (Figure B-1).

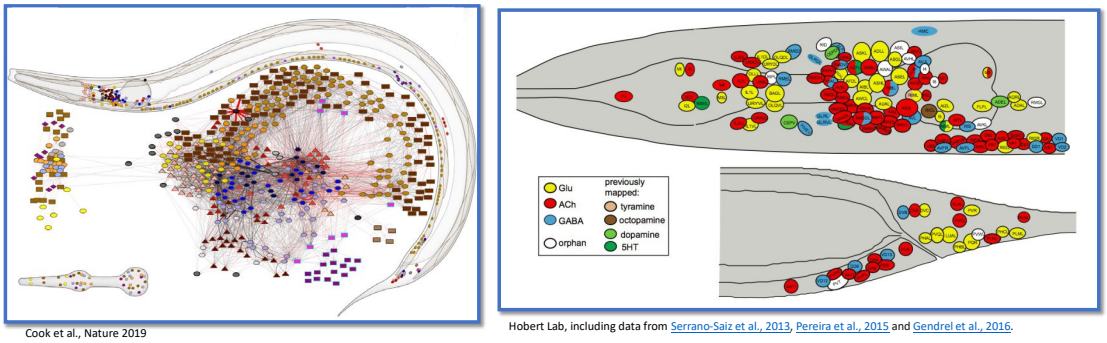

Figure B-1: Graphical displays of C. elegans neurobiology.

(A) The physical connectome. The approximate location of every neuron cell body, processes, and physical synapses.(Cook et al. 2019) (B) The neurotransmitter atlas. The neurons that release each of the C. elegans neurotransmitter that are known. (Serrano-Saiz et al. 2013; Gendrel et al. 2016)

Even so, a remaining challenge to fully exploiting these data sets is the inability to easily identify individual neurons. Though the transparent body of *C. elegans* naturally gives

way to fluorescent microscopy—it is not easy to identify the neurons that express the fluorescent marker. Reasons for this include that neurons that are near each other often have similar morphologies, making it hard to distinguish them from neighboring cells and animal to animal variability in the 3D positioning of neurons. In addition, microscopy techniques often compress and distort 3D image in a way that makes it unintuitive to fully consider the 3D neuro-landscape of the animal, rendering it more difficult to observe symmetries and landmarks crucial for identifying classes of neurons form one another.

NeuroPAL (Neuronal Polychromatic Atlas of Landmarks; Yemini et al. 2021) was developed recently to address some of these issues. Utilizing 41 overlapping neuron-specific reporters, the NeuroPAL transgene expresses a cell-specific combination of three distinguishable fluorescent proteins and a pan-neuronal marker (Figure B-2). The combinatorial promoters work so that, much like pixels, each cell expresses a different amount of red, green, and blue fluorophore resulting in nearby cells being distinguishable from one another by the combination of fluorescence. Additionally, since each of the NeuroPAL fluorophores are distinct from GFP, animals carrying the NeuroPAL transgene can be crossed or injected with GFP markers for study, making identification of neurons easier than previous methods, which usually involved using markers for a particular class of neurons such as *cho-1::mCh*, which expressed in all cholinergic neurons (Figure B-3).

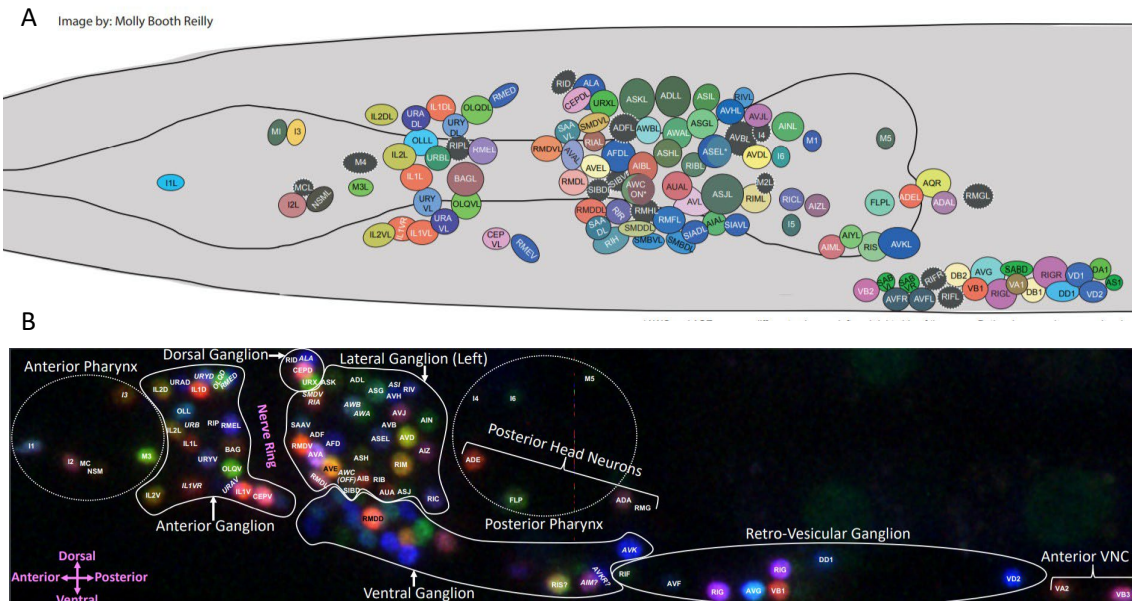

Figure B-2: NeuroPAL colors neurons uniquely using a combinatorial promoter.

(A) Cartoon diagram of *C. elegans* from a lateral view, annotating the approximate position of each neuron's nucleus and the color the NeuroPAL transgene produces. (B) A confocal image of a NeuroPAL animal (Yemini et al. 2019).

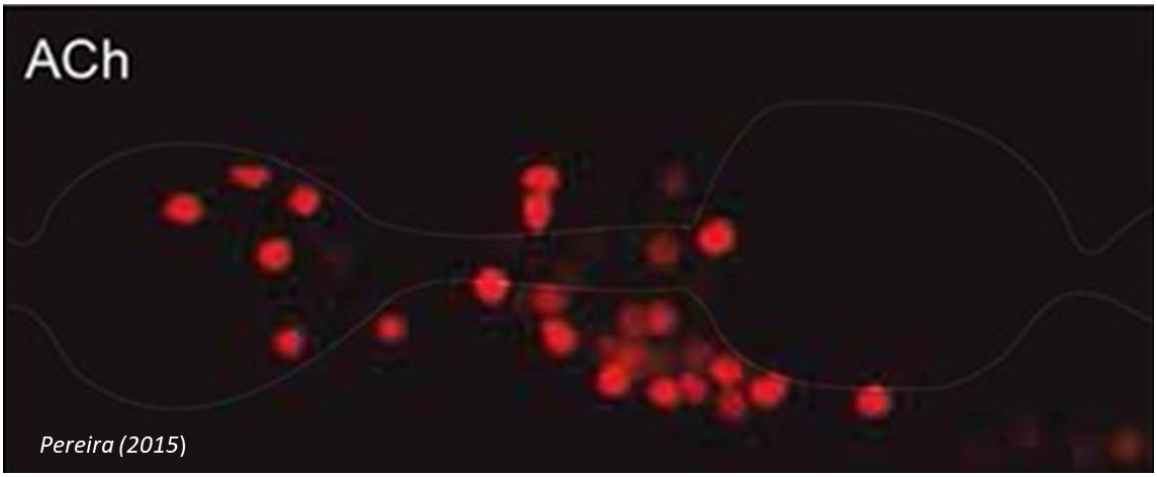

Figure B-3: Example of neurotransmitter class marker (cho-1::mCh).

In this example, cholinergic neurons, that were previously the standard for C. elegans cell IDs are displayed in red via the expression of *cho-1* tagged with mCherry in a fosmid. White lines denotate the pharyngeal bulb (Pereira et al. 2015).

The Koelle lab initially planned to use this new technology to complete another layer of mapping that would detail each GPCR expressed by each *C. elegans* neuron. The lab soon discovered, however, that as promising of a tool as NeuroPAL is, it is still in the early stages with many barriers to its use. Therefore, the lab pivoted its goal to being able to better understand how to use NeuroPAL as a tool itself. I sought out to devise a system to use NeuroPAL while addressing the challenges described below. All work mentioned below was completed alongside my labmates, Emerson Santiago and Ashish Shelar, PhD, unless otherwise specified.

Challenges to NeuroPAL

Neuroanatomy

First, utilizing NeuroPAL requires a lot of experience in *C. elegans* neuroanatomy and nomenclature. While small, the worm is a 3D animal and therefore the neurons are positioned in 3D space along the left/right, dorsal/ventral, and lateral/medial axes (much like an x/y/z coordinate system). The 302 *C. elegans* neurons have been grouped into 118 classes, which usually express the same genes (Hsieh et al. 2014; Chuang and Bargmann 2005)—an important consideration, when the using promoters of genes of interest to study expression. Most of these neurons are found in left(L)/right(R) pairs (e.g., the RIP neurons, with RIPL and RIPR); but some come in groups of four of left(L)/right(R) and dorsal(D)/ventral(V) (e.g., the OLQ neurons, with OLQDL, OLQDR, OLQVL, and OLQVR); or even six (e.g., the IL2 neurons, with IL2L, IL2R, IL2DL, IL2DR, IL2VL, and IL2VR). Conversely, some classes only have one neuron member, who can sometimes be found along the medial cross section (e.g., I3), but others can asymmetrically lean to the left or right (e.g., AQR).

The vast majority of neurons (181/302) reside in the head, where they are organized into seven loosely-defined clusters for which the boundaries are unclear: the anterior ganglion anterior bulb (AGAB), anterior ganglion post bulb (AGPB), dorsal ganglion (DG), lateral

ganglion (LAG), ventral ganglion (VG), retro-vesicular ganglion (RVG), and posterior head (PH) neurons. Following the length of the animal from anterior to posterior, 84 neurons—mostly consisting of motor cord neurons that function primarily in locomotion—are found along the ventral nerve cord (VNC), a dense axon tract comparable in function to a spinal cord. This is also where the neurons involved in the *C. elegans* egg-laying system are located. Continuing posteriorly at the tail, 45 neurons are loosely organized into three regions: the preanal ganglion (PAG), the dorso-rectal ganglion (DRG), and the lumbar ganglion (LUG). (Figure B-4)

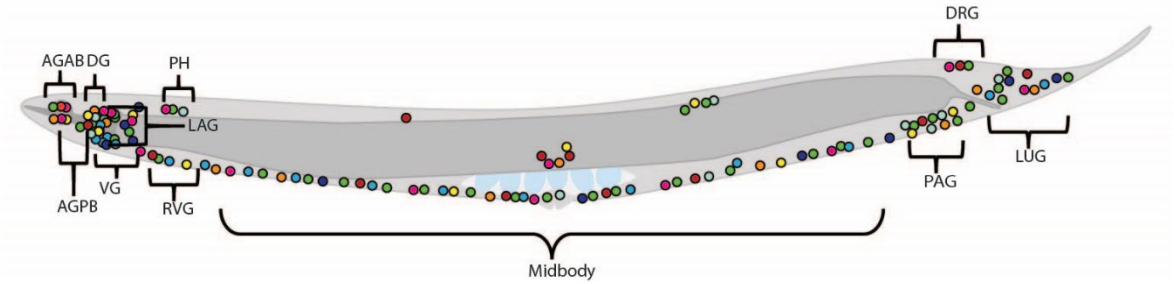

Figure B-4: Clusters of neurons in C. elegans.

The location of *C. elegans* neural clusters, including seven in the head and three in the tail. *AGAB= Anterior Ganglion, Anterior Bulb; AGPB = Anterior Ganglion, Posterior Bulb; DG = Dorsal Ganglions, VG = Ventral Ganglions, PH = Posterior Head; LAG = Lateral Anterior Ganglion; RVG = Retrovesticular Ganglion; PAG = pre-anal ganglion, LUG= Lumbar Ganglion, and DRG = Dorsorectal ganglion*

Understanding the canonical relative relationship between neurons along the three axes, as well as their approximant relationship to other physical layers of the worm (e.g., cuticle, muscles, pseudocoelom) and structures in the anatomy (e.g., the pharyngeal bulbs, the vulva, the anus) are all crucial to correctly identifying neurons.

Imaging

The first challenge to imaging is the technical aspect and the high learning curve of operating the microscope and software itself. The microscopes have a bevy of features that frequently feel redundant. For example, turning up either the laser intensity, gain, or the

exposure will all increase the strength of a signal; however, they all do so differently. The laser intensity increases the strength of the laser; the gain increases the amplification applied to the signal once detected; and the exposure is how long the laser is applied to the sample and the emission spectra summed over. Increasing the exposure and laser intensity can increase the risk of bleaching samples, whereas increasing the gain enhances any background noise and therefore different adjustments to these setting can result in different images. With multiple fluorescent signals, as in the case of NeuroPAL, this problem is exponentially amplified. Bleed-through, in which the emission of one fluorophore is detected in a channel designated for another fluorophore, increases as more channels are added. Furthermore, turning one laser up higher relative to others could compromise the end combination of colors that create the crucial 'unique pixel' necessary for NeuroPAL. Imaging in animals causes a wide amount of variation. Some animals simply express signal better or worse and therefore all settings still have to be quickly optimized for each individual animal to avoid the animal bleaching or desiccating.

The images collected need to have a high enough resolution and sensitivity to visualize the desired target but done at a speed in which a significant quantity of images can be collected. In microscopy, a principle called the "Imaging Triangle of Compromise" (Zeiss 2019) describes a conundrum among resolution, speed, and sensitivity (Figure B-5). For any given signal-to-noise ratio, improving any of those conditions will come at the cost of at least one of the others. For the data to be collected, the imaging resolution needs to be of a sufficient quantity to distinguish cells from one another; the sensitivity needs to be sufficient to visualize dimmer cells or cells further from the microscope that experience fading across the z-axis; and the speed needs to be fast enough to collect the data before the sample starts degrading and collect a sufficient *n*-number of samples to account for individual variation.

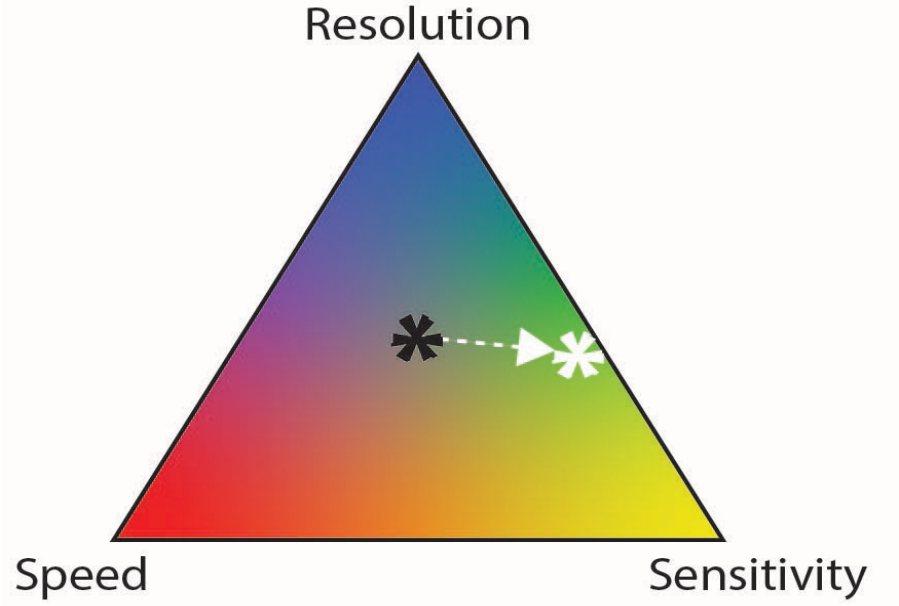

Figure B-5: The Imaging Triangle of Compromise in which resolution, speed, and sensitivity are at odds with each other, and any gain in one respect compromises another.

.

Data Organization

To manage the identification of 302 cells in a 3D space was challenging when working with multiple scientists. When some groups use NeuroPAL, interest might be restricted to a small region of the *C. elegans*; however, even these regions can be difficult to analyze. For example, the head of the *C. elegans* contains nearly 200 neurons to sort, organize, and distinguish. Additionally, while the data is captured in 3D z-stacks, images are usually examined in 2D slices, which can make visualizing the 3D relationship, a crucial component of distinguishing cells from one another, difficult.

It is important to have a system to keep track of each neuron to avoid missing or duplicating neurons. In addition, when considering scoring and quantification (i.e., 'does this cell express GFP') there is a wide-range of human error. That is to say, one scientist could consider the GFP signal "strong," another "moderate," and another "weak" due to individual bias or computer settings used to view the image. While software like ImageJ can quantify signal, the software itself is contingent upon the imaging conditions used and therefore the individual animals.

My goal in the NeuroPAL project was to develop methods to overcome the challenges mentioned above and streamline the use of NeuroPAL in the Koelle lab.

Imaging Conditions

The first step of developing a system for our lab to use NeuroPAL was to develop general imaging conditions that could show NeuroPAL in sufficient resolution to identify cells. These conditions could be used later to answer questions that required the identifying of promoter-GFP fusions for genes of interest.

As previously mentioned, the Koelle Lab was originally interested in NeuroPAL to complete a GPCR atlas for the entire organism. 17/26 *GPCR::GFP* x NeuroPAL lines had already been crossed and made homozygous. After briefly examining each line to establish a baseline of what to expect in NeuroPAL x GFP lines, I decided to use the *dop-4::SL2::GFP* x NeuroPAL strain LX2753 (*otIs670; vsIs287*) as a case-study with 'normal' GFP brightness and the *ser-4::GFP* x NeuroPAL LX2735 (*otIs670; ljIs570*) as a case-study for high GFP brightness.

Using the metrics suggested by Yemini (2019a) as a guideline and the two case study *C. elegans* lines I selected, I used the Zeiss 880 to develop baseline imaging conditions for NeuroPAL. The conditions listed in Table B-1 describe the optimization of the following:

1) signal-to-noise of the NeuroPAL markers
2) signal-to-noise of the GFP markers
3) minimal bleed through between markers
4) time-efficiency
5) brightfield channel to examine neuronal positioning within the context of the whole animal

Table B-1: Microscope Settings for Low and High GFP.

Microscope settings were created to optimize the triangle of compromise and develop images with high enough resolution and sensitivity to view all the neurons, while also collecting images quickly enough to facilitate the data collection of the animals needed.

Tracks

Low GFP *6.15 – 8.20 (min)* / High GFP* *9.15 – 11.27 (min)*	1		2		3	
					3*	4*
Reporter	TagRFP-T	Brightfield	mTagBF2	mNeptune 2.5	CyOFP	Reporter GFP
Intensity	30 – 45	—	10 – 20	40 – 50	30 – 55	25 – 45
Gain	600 – 650	125 – 175	550 – 600	650 – 700	600 – 750	600 – 750
Laser Line	561	—	405	594	488	488
Excitation (nm)	561	—	405	590-640	488	488
Emission boundaries (nm)	565 – 600	—	410 – 470	600	520	490 – 520

The resulting imaging conditions have 6 channels: brightfield, a pan-neuronal marker, a blue (mTagBF2), a red (mNeptune2.5), a green marker (CyOFP), and the reporter GFP. The imaging conditions are set up in either in 3-4 tracks. If the image has low-or-normal GFP brightness, the GFP can be excited at the same time as the CyOFP. However, if the GFP brightness is incredibly high, then the GFP and CyOFP have to be separated into two different tracks, and the laser intensity of the GFP has to be on the low end of the intensity range.

The NeuroPAL channels bleach rapidly, so to capture useful images the adjustment for each setting could only take a few seconds per animal. Longer adjustments, like orienting the animal within the frame, could only happen with the brightfield channel.

3D Atlas Creation

The next step in developing a system to identify cells using NeuroPAL was to determine how the images would be analyzed and the data would be recorded. Yemini (2019a) recommend using ImageJ to 'slide' through 2D z-slices. We felt that a 3D view would help overcome some of the challenges discussed above; including the relationship across neuron pairs that are crucial for identification; the relative positioning across the z-axis; and the colocalization of GFP. While ImageJ does have a 3D projection feature, we found that this feature took excessive time to load and was not intuitive to use. I decided that BitPlane's IMARIS software would be an excellent choice for annotating NeuroPAL images. Z-stacks would load in 3D and a native annotation feature allows any 3D voxel to be labeled. Viewpoints can be easily toggled between 3D and 2D slices, which gave us both the whole 3D structure as well as the precision of 2D slices.

To develop a simplified, accessible way to use NeuroPAL, we decided it would be necessary to create a 3D atlas of NeuroPAL within IMARIS that consolidated the entire identification process into one image. Downloading the 3-D reference file of a NeuroPAL

animal (Yemini 2019b), and using Yemini's guide as well as other tools and databases, myself and another labmate, Ashish Shelar, set to work on IDing the cells. We felt it was important to have more than one person prepare the Atlas to minimize user-to-user error.

For each region, we independently annotated the same image. Before this, I developed a spreadsheet to help keep track of the neurons as we labeled them in IMARIS (Table B-2). In this spreadsheet, neuron classes were sorted by the ganglion in an anterior to posterior fashion, and alphabetically within each ganglion. The neurons were also color coded by what the expected NeuroPAL color would be. As annotations were made in IMARIS, we wrote down the cells we labeled and the excel sheet counted the times each cell was mentioned and conditionally formatted if a cell class was over/underrepresented. I focused on neuron class (e.g., I1) instead of specific neuron (e.g., I1L or I1R) because in a lot of cases the left vs right was apparent, and in cases where they weren't (e.g., is this the dorsal left or just the left) labeling them by class alone helped reduce discrepancies. When the cell was identified, the identity was written in column B. Alternatively, we could check off individual neurons in column L.

Throughout this project, excel tables were preferred over more sophisticated software/programming., so that its use would not be limited by our ability to program.

Table B-2: Neuron tracker sheet for cell IDs.

Screenshot of spreadsheet designed to track annotations in IMARIS to create a 3D neuron atlas. Users entered in their annotations in Column B "ID" where in would be matched to a given class (column E) and counted in column G via the equation " =SUM(COUNTIFS(B:B, E4&"*"))". This was so users did not have to know which subclass of neuron each annotation was. Column G was conditionally formatted to be colored orange should there be less than the number of members in a neuron class (e.g., in the figure, there are no MI cells annotated where there should be 1, so it is colored orange) or yellow if there are too many annotations (e.g., the ALA neurons). A full list of individual neurons is found in column L. Locations are listed in columns D and K, and the cell classes are formatted to be the approximate color that they are found to have in NeuroPAL. Red candy stripe (e.g., MC) mean invisible and only seen by pan-neuronal marker.

	A	B	C	D	E	F	G	H	I	J	K	L
1				**Neurons by Class**							**Individual Neurons**	
2	Ann #	ID		Location	Class	Expected	Counted				Location	Cell
3	1	M3L				302	6				AGAB	I1L
4	2	M3R		AGAB	I1	2					AGAB	I1R
5	3	ALA		AGAB	I2	2	0				AGAB	I2L
6	4	ALA		AGAB	I3	1	0				AGAB	I2R
7		AVER		AGAB	M3	2	2				AGAB	I3
8		AVER		AGAB	M4	1	0				AGAB	M3L
9				AGAB	MC	2	0				AGAB	M3R
10				AGAB	MI	1	0				AGAB	M4
11				AGAB	NSM	2	0				AGAB	MCL
12				AGPB	BAG	2	0				AGAB	MCR
13				AGPB	IL1	6	0				AGAB	MI
14				AGPB	IL2	6	0				AGAB	NSML
15				AGPB	OLL	2	0				AGAB	NSMR
16				AGPB	OLQ	4	0				AGPB	BAGL
17				AGPB	RIP	2	0				AGPB	BAGR
18				AGPB	RME	4	0				AGPB	CEPVL
19				AGPB	URA	4	0				AGPB	CEPVR
20				AGPB	URB	2	0				AGPB	IL1DL
21				AGPB	URY	4	0				AGPB	IL1DR
22				DG	ALA	1	2				AGPB	IL1L
23				DG	CEP	4	0				AGPB	IL1R
24				DG	RID	1	0				AGPB	IL1VL
25				DG	URX	2	0				AGPB	IL1VR
26				LAG	ADF	2	0				AGPB	IL2DL
27				LAG	ADL	2	0				AGPB	IL2DR
28				LAG	AFD	2	0				AGPB	IL2L
29				LAG	AIB	2	0				AGPB	IL2R
30				LAG	AIN	2	0				AGPB	IL2VL
31				LAG	AIZ	2	0				AGPB	IL2VR
32				LAG	ASE	2	0				AGPB	OLLL
33				LAG	ASG	2	0				AGPB	OLLR
34				LAG	ASH	2	0				AGPB	OLQDL
35				LAG	ASI	2	0				AGPB	OLQDR
36				LAG	ASI	2	0				AGPB	OLQVL

Simultaneously in IMARIS, each of us independently labeled the voxels in the 3D image corresponding to what we considered to be the center of the cell. Then, the two annotations were overlapped in IMARIS by importing one set over the other and manually compared (Table B-3). For cells on which both of us agreed for the ID, it was considered 'verified' and labeled accordingly. On the other hand, neurons on which we did not agree were labeled according to below, and the discrepancy was described. Discrepancies usually fell into the following categories, an example of which can be seen in Figure B-6:

1) Different IDs: both of us agree it is a neuron, but disagree on the ID of the neuron.
2) Labeled vs not labeled: either one of us did not consider the region in question a neuron or were so uncertain as to its ID that it was not labeled. This happened frequently with faint neurons. This was also a problem with dense regions; sometimes, one of us considered a region of voxels one neuron, while the other considered it two neurons.
3) Left vs right: the neuron ID is agreed upon, but the side is not.

   While there are asymmetrical neurons (e.g., ASQ) that are only found on one side of the animal, there were disagreements on which side of the animal we were viewing in the 3D image.
4) Misaligned center: both the users agree on the cell and the IDs, but disagree on the center of the nucleus.

   This was important for dense neuron regions, where misaligning the center of one neuron could result in missing another neuron completely.
5) Repeat: despite best efforts, a cell ID was given more than once.

A list of remaining discrepancies, or variations, was generated, and each of us compared the discrepancy to the verified cells and attempted to redo the remaining IDs, reducing the variations in an iterative process. A spreadsheet took the annotations from the discrepancies

table and automatically sorted verified neurons and neurons that had yet to be conclusively identified (Table B-4).

Table B-3: Variant spreadsheet of disagreed upon neuron IDs

Screenshot of an Excel sheet I created to compare NeuroPAL annotations. After our annotations were combined on one IMARIS file, the annotations would be manually compared and noted on this spreadsheet. A 'Y' would indicate that they agree; 'Atlas?' confirms that with the ID be agreed upon, the cell is entered correctly into the 3D atlas; "R" refers to "revised" in the case of an ID disagreement. Cells are conditionally-formatted to be highlighted Green if agreed upon, red if disagreed upon, and yellow for other issues. For IDs in which there is a disagreement or variation, each scientist explained their annotation

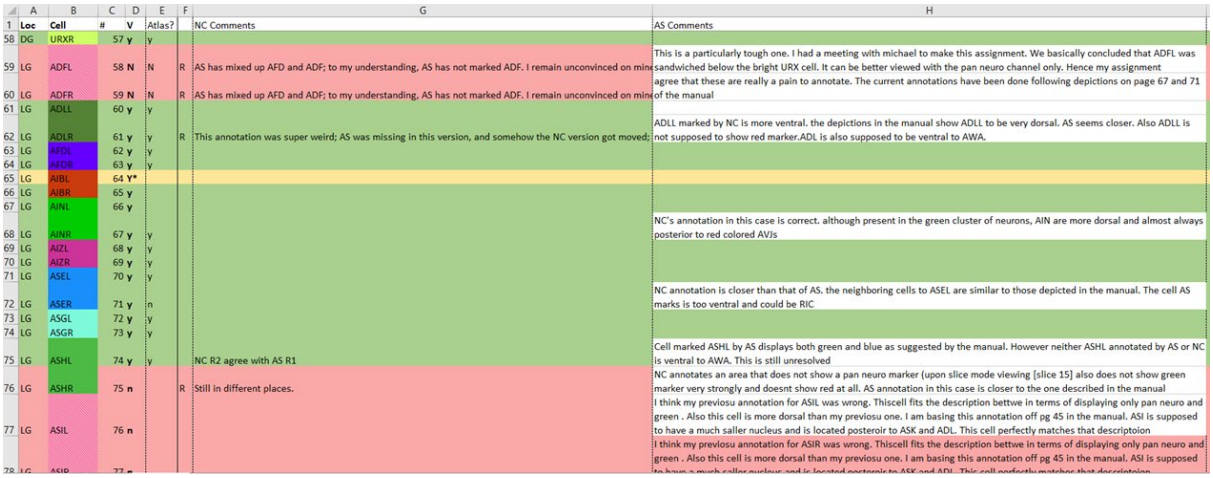

	A	B	C	D	E	F	G	H
1	**Loc**	**Cell**	**#**	**V**	Atlas?		NC Comments	AS Comments
58	DG	URXR	57	y	y			
59	LG	ADFL	58	N	N	R	AS has mixed up AFD and ADF; to my understanding, AS has not marked ADF. I remain unconvinced on mine	This is a particularly tough one. I had a meeting with michael to make this assignment. We basically concluded that ADFL was sandwiched below the bright URX cell. It can be better viewed with the pan neuro channel only. Hence my assignment
60	LG	ADFR	59	N	N	R	AS has mixed up AFD and ADF; to my understanding, AS has not marked ADF. I remain unconvinced on mine	agree that these are really a pain to annotate. The current annotations have been done following depictions on page 67 and 71 of the manual
61	LG	ADLL	60	y	y			
62	LG	ADLR	61	y	y	R	This annotation was super weird; AS was missing in this version, and somehow the NC version got moved;	ADLL marked by NC is more ventral. the depictions in the manual show ADLL to be very dorsal. AS seems closer. Also ADLL is not supposed to show red marker.ADL is also supposed to be ventral to AWA.
63	LG	AFDL	62	y	y			
64	LG	AFDR	63	y	y			
65	LG	AIBL	64	Y*				
66	LG	AIBR	65	y				
67	LG	AINL	66	y				
68	LG	AINR	67	y	y			NC's annotation in this case is correct. although present in the green cluster of neurons, AIN are more dorsal and almost always posterior to red colored AVJs
69	LG	AIZL	68	y	y			
70	LG	AIZR	69	y	y			
71	LG	ASEL	70	y	y			
72	LG	ASER	71	y	n			NC annotation is closer than that of AS. the neighboring cells to ASEL are similar to those depicted in the manual. The cell AS marks is too ventral and could be RIC
73	LG	ASGL	72	y	y			
74	LG	ASGR	73	y	y			
75	LG	ASHL	74	y	y		NC R2 agree with AS R1	Cell marked ASHL by AS displays both green and blue as suggested by the manual. However neither ASHL annotated by AS or NC is ventral to AWA. This is still unresolved
76	LG	ASHR	75	n		R	Still in different places.	NC annotates an area that does not show a pan neuro marker (upon slice mode viewing [slice 15] also does not show green marker very strongly and doesnt show red at all. AS annotation in this case is closer to the one described in the manual
77	LG	ASIL	76	n				I think my previosu annotation for ASIL was wrong. Thiscell fits the description bettwe in terms of displaying only pan neuro and green . Also this cell is more dorsal than my previosu one. I am basing this annotation off pg 45 in the manual. ASI is supposed to have a much saller nucleus and is located posteroir to ASK and ADL. This cell perfectly matches that descriptoion
78	LG	ASIR	77	n				I think my previosu annotation for ASIR was wrong. Thiscell fits the description bettwe in terms of displaying only pan neuro and green . Also this cell is more dorsal than my previosu one. I am basing this annotation off pg 45 in the manual. ASI is supposed to have a much saller nucleus and is located posteroir to ASK and ADL. This cell perfectly matches that descriptoion

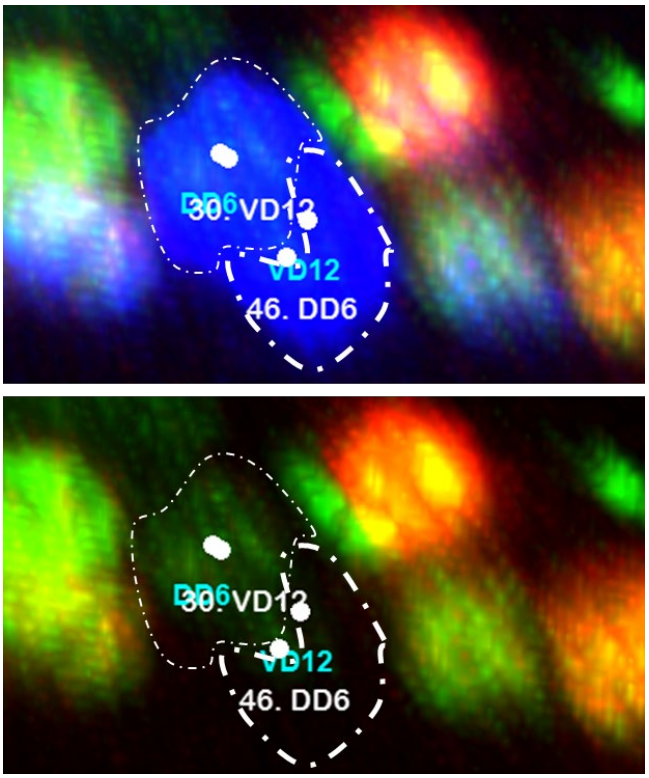

Figure B-6: Two annotated labels of two cells in which the two scientists disagree.

An example of two annotated labels in which there is a disagreement on the cell ID.

Table B-4: Screenshot of table generated of both verified and disagreed upon neuron IDs

Screenshot of an excel spreadsheet on which information from the table depicted on Table B-3 was sorted and labeled into either 'verified' neurons (Columns A-D) or cells in which their identity varied between Ashish and myself. In each case, the lists were sorted by an array equation that would automatically update as the variations were resolved on the manual notes. :=IF(ISERROR(INDEX('CellStatus'!$A$2:$D$178,SMALL(IF(COUNTIF($B$2,'CellStatus'!$D$2:$D$178),MATCH(ROW('CellStatus'!$A$2:$D$178),ROW('CellStatus'!$A$2:$D$178)),""),ROWS('CellStatus'!$H2:K$2)),COLUMNS('CellStatus'!$A$1:D1)))=TRUE,"",INDEX('CellStatus'!$A$2:$D$178,SMALL(IF(COUNTIF($B$2,'CellStatus'!$D$2:$D$178),MATCH(ROW('CellStatus'!$A$2:$D$178),ROW('CellStatus'!$A$2:$D$178)),""),ROWS('CellStatus'!$H2:K$2)),COLUMNS('CellStatus'!$A$1:D1)))

	A	B	C	D	E	F	G
1	Summary		188		Discrepencies		
2	Verified	Y	142		N	46	
3	Y.P	Y*					
4	Location	Cell	#	Status		Location	Cell
5	AGAB	I1L	1	Y		AGPB	RIPL
6	AGAB	I1R	2	Y		AGPB	RIPR
7	AGAB	I2L	3	Y		LG	ADFL
8	AGAB	I2R	4	Y		LG	ADFR
9	AGAB	I3	5	Y		LG	ASHR
10	AGAB	M3L	6	Y		LG	ASIL
11	AGAB	M3R	7	Y		LG	ASIR
12	AGAB	M4	8	Y		LG	ASJL
13	AGAB	MCL	9	Y		LG	ASJR
14	AGAB	MCR	10	Y		LG	AVBL
15	AGAB	MI	11	y		LG	AVBR
16	AGAB	NSML	12	Y		LG	AVKL
17	AGAB	NSMR	13	Y		LG	AWAL
18	AGPB	BAGL	14	y		LG	AWCL
19	AGPB	BAGR	15	Y		LG	AWCR
20	AGPB	CEPVL	16	Y		LG	RIAR
21	AGPB	CEPVR	17	Y		LG	RIS
22	AGPB	IL1DL	18	y		VG	AIAL
23	AGPB	IL1DR	19	y		VG	AIAR
24	AGPB	IL1L	20	y		VG	AIML
25	AGPB	IL1R	21	y		VG	AIYL
26	AGPB	IL1VL	22	y		VG	RMFR
27	AGPB	IL1VR	23	y		VG	SIAVL
28	AGPB	IL2DL	24	y		VG	SIAVR
29	AGPB	IL2DR	25	y		VG	SIBDL
30	AGPB	IL2L	26	y		VG	SIBDR
31	AGPB	IL2R	27	y		VG	SIBVL
32	AGPB	IL2VL	28	Y*		VG	SIBVR
33	AGPB	IL2VR	29	y		VG	SMBDL
34	AGPB	OLLL	30	y		VG	SMBDR
35	AGPB	OLLR	31	y		VG	SMBVL
36	AGPB	OLQDL	32	y		VG	SMBVR

For the midbody and tail, in which there are fewer neurons, the process was straightforward with only one round of revisions. However, the neurons in the head were more difficult. There are a greater in number of them and they are denser, and even with NeuroPAL's combination pixel effect, many cells, particularly in the lateral anterior ganglion (LAG) and ventral ganglion (VG), were similarly colored, making it difficult to distinguish neuron classes from one another and neuron nuclei from one another. It took six rounds to agree on the IDs of 60% of the 181 cells in the head, and over 12 rounds to fully come to a consensus and completed the 3-D Neuron Atlas (Figure B-7).

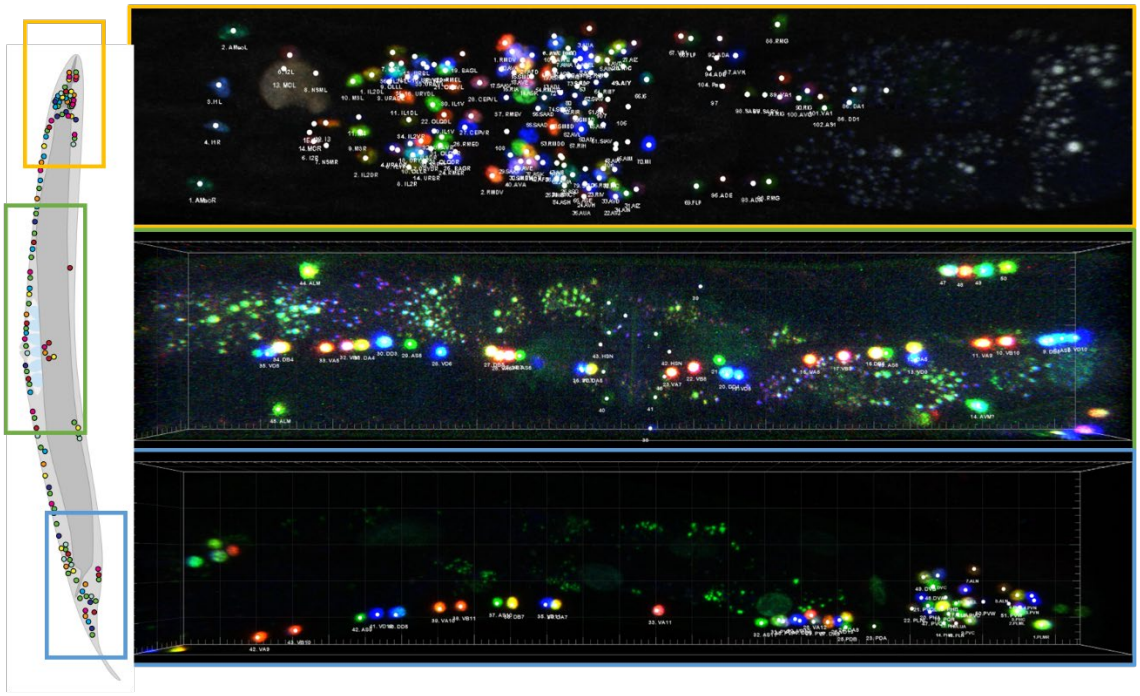

Figure B-7: 2-D Images of each of the 3-D NeuroPAL neuron atlases.

Top: head neurons, middle: midbody neurons, bottom: tail neurons. Images displayed using IMARIS.

GFP Scoring

The final step was to run a pilot for NeuroPAL to identify GFP-expressing cells. I continued to use the DOP4 x NeuroPAL and SER4 x NeuroPAL. I used these two strains to determine the *n*-number (*n*=5) and the orientation of images (2x lateral, 3x dorsal/ventral) that would be needed to confidently identify GFP-expressing neurons (Figure B-8). Multiple animal orientations are necessary in order to combat the fading across the z-axis.

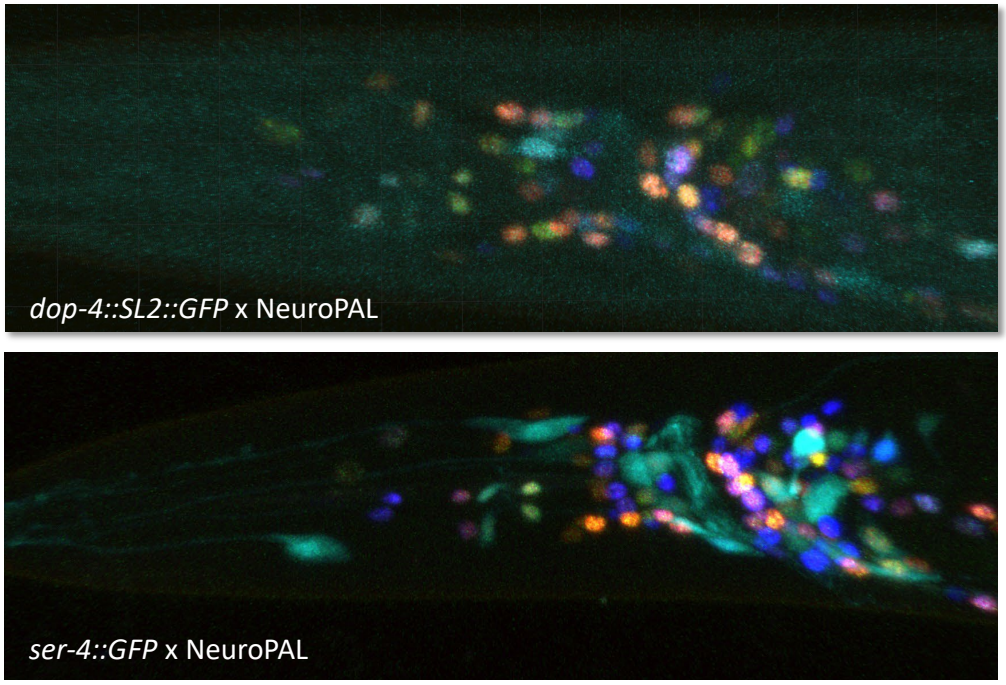

Figure B-8: GPCR::GFP x NeuroPAL pilot lines.

(Top) *dop-4::SL2::GFP* x NeuroPAL worm head example. (Bottom) *ser-4::GFP* x NeuroPAL worm head example. Using the 3D NeuroPAL atlas described earlier, cells that co-express GFP can be easily identified and scored.

Similar to how we created the 3D atlas, we decided that each image should be scored by at least two scientists. I built another spreadsheet, in which we scored which cells were expressing GFP and how brightly. GFP-expressing cells were labeled on a 1-3 scale, with 1 being barely visible above background; 2 being adequate expression; and 3 being among the brightest of GFP-expressing cells (Table B-5). The scoring sheets from each scientist were then combined into a sheet that automatically calculated the average score, alerted if the score between the two individuals was more than 0.5, and categorized the expression as weak, strong, variable, or anomalous (Table B-6). We described variability as if a cell is GFP positive more than once, but less than half of the time, and anomalous as when a cell is strongly GFP positive, but only once. The final list of GFP positive cells identified are displayed in Table B-7.

The imaging parameters, software analysis, and excel sheets that I created were fundamental in the Koelle lab's successful use of NeuroPAL and the submitted publication by Santiago et al (2022).

Table B-5: Scoring Sheet for GPCR::GFP expression pilots

Screenshot of Excel spreadsheet on which each scientist would fill out the sheet, ranking neurons according to GFP brightness (1 = barely above background; 2 = sufficiently/typically bright; 3 = among the brightest). The cells would conditionally format to mirror the ranking. Neurons not expressing GFP were left blank.

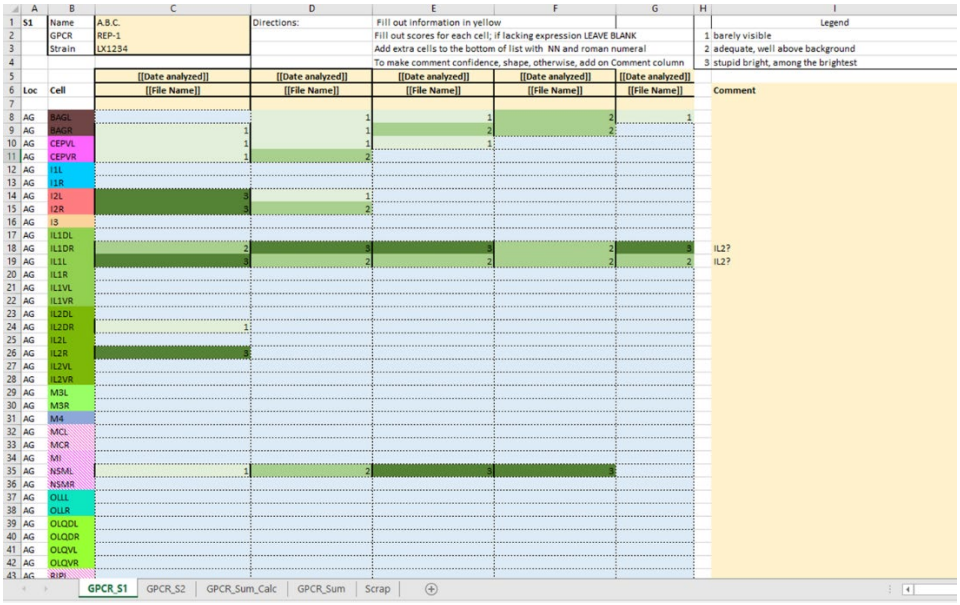

	A	B	C	D	E	F	G	H	I
1	S1	Name	A.B.C.	Directions:	Fill out information in yellow				Legend
2		GPCR	REP-1		Fill out scores for each cell; if lacking expression LEAVE BLANK				1 barely visible
3		Strain	LX1234		Add extra cells to the bottom of list with NN and roman numeral				2 adequate, well above background
4					To make comment confidence, shape, otherwise, add on Comment column				3 stupid bright, among the brightest
5			[[Date analyzed]]	[[Date analyzed]]	[[Date analyzed]]	[[Date analyzed]]	[[Date analyzed]]		
6	Loc	Cell	[[File Name]]	[[File Name]]	[[File Name]]	[[File Name]]	[[File Name]]		Comment
7									
8	AG	BAGL		1	1	2	1		
9	AG	BAGR	1	1	2	2			
10	AG	CEPVL	1	1	1				
11	AG	CEPVR	1	2					
12	AG	I1L							
13	AG	I1R							
14	AG	I2L	3	1					
15	AG	I2R	3	2					
16	AG	I3							
17	AG	IL1DL							
18	AG	IL1DR	2	3	3	2	3		IL2?
19	AG	IL1L	3	2	2	2	2		IL2?
20	AG	IL1R							
21	AG	IL1VL							
22	AG	IL1VR							
23	AG	IL2DL							
24	AG	IL2DR	1						
25	AG	IL2L							
26	AG	IL2R	3						
27	AG	IL2VL							
28	AG	IL2VR							
29	AG	M3L							
30	AG	M3R							
31	AG	M4							
32	AG	MCL							
33	AG	MCR							
34	AG	MI							
35	AG	NSML	1	2	3	3			
36	AG	NSMR							
37	AG	OLLL							
38	AG	OLLR							
39	AG	OLQDL							
40	AG	OLQDR							
41	AG	OLQVL							
42	AG	OLQVR							
43	AG	RIPL							

GPCR_S1 | GPCR_S2 | GPCR_Sum_Calc | GPCR_Sum | Scrap

Table B-6: Combined Scoring Sheet Calculations

Screenshot of the Excel sheet on which the two scientists' individual scoring sheets (see Table B-5) were automatically averaged by this spreadsheet that calculated the average brightness, and from this calculation determined if expression was strong (>1.5), weak (1.5>x>0.6), or not expressed (0.6>x). The formula also accounted for variability—that is, if a cell is GFP positive more than once, but less than half of the time, or anomalous, in which a cell is strongly GFP positive, but only once. This was done with the following formula:

=IFERROR(IF(AND((IF((COUNTIF(Z9:AD9,""))>=3,1,0)),IF((COUNTIF(Z9:AD9,1)+COUNTIF(Z9:AD9,1.5)+(COUNTIF(Z9:AD9,2)+COUNTIF(Z9:AD9,2.5)+COUNTIF(Z9:AD9,3)))>=2,1,0)),"Variable",IF(AND((IF((COUNTIF(Z9:AD9,""))>=3,1,0)),IF(((COUNTIF(Z9:AD9,2)+COUNTIF(Z9:AD9,2.5)+COUNTIF(Z9:AD9,3)))>=1,1,0)),"ANOMALY",IF(AVERAGE(Z9:AD9)>=1.5,"Strong",IF(AVERAGE(Z9:AD9)>=0.6,"Weak","No")))),"")

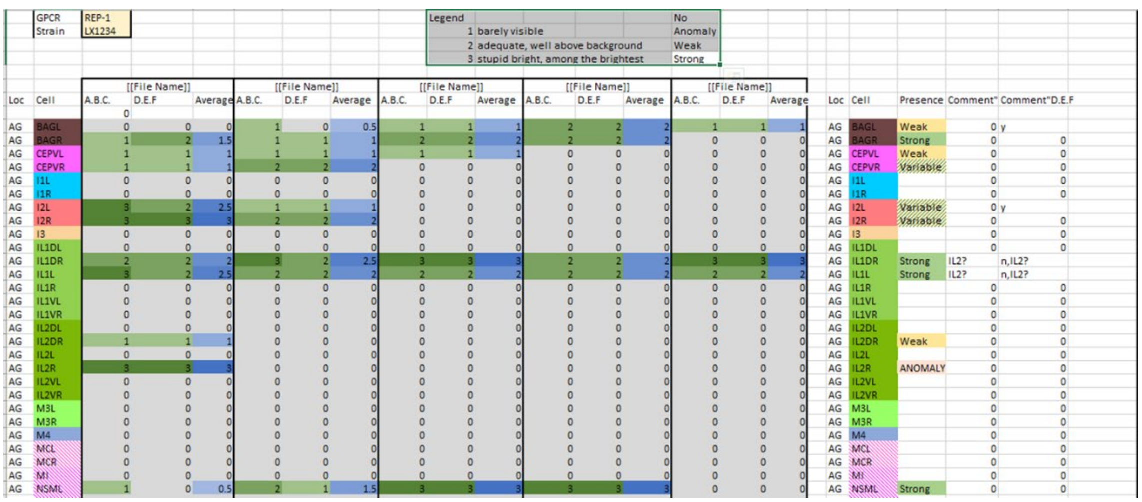

GPCR	REP-1		Legend			No
Strain	LX1234		1	barely visible		Anomaly
			2	adequate, well above background		Weak
			3	stupid bright, among the brightest		Strong

		[[File Name]]			[[File Name]]			[[File Name]]			[[File Name]]			[[File Name]]							
Loc	Cell	A.B.C.	D.E.F	Average	A.B.C.	D.E.F	Average	A.B.C.	D.E.F	Average	A.B.C.	D.E.F	Average	A.B.C.	D.E.F	Average	Loc	Cell	Presence	Comment"	Comment"D.E.F
		0																			
AG	BAGL	0	0	0	1	0	0.5	1	1	1	2	2	2	1	1	1	AG	BAGL	Weak	0	y
AG	BAGR	1	2	1.5	1	1	1	2	2	2	2	2	2	0	0	0	AG	BAGR	Strong	0	0
AG	CEPVL	1	1	1	1	1	1	1	1	1	0	0	0	0	0	0	AG	CEPVL	Weak	0	0
AG	CEPVR	1	1	1	2	2	2	0	0	0	0	0	0	0	0	0	AG	CEPVR	Variable	0	0
AG	I1L	0	0	0	0	0	0	0	0	0	0	0	0	0	0	0	AG	I1L		0	0
AG	I1R	0	0	0	0	0	0	0	0	0	0	0	0	0	0	0	AG	I1R		0	0
AG	I2L	3	2	2.5	1	1	1	0	0	0	0	0	0	0	0	0	AG	I2L	Variable	0	y
AG	I2R	3	3	3	2	2	2	0	0	0	0	0	0	0	0	0	AG	I2R	Variable	0	0
AG	I3	0	0	0	0	0	0	0	0	0	0	0	0	0	0	0	AG	I3		0	0
AG	IL1DL	0	0	0	0	0	0	0	0	0	0	0	0	0	0	0	AG	IL1DL		0	0
AG	IL1DR	2	2	2	3	2	2.5	3	3	3	2	2	2	3	3	3	AG	IL1DR	Strong	IL2?	n,IL2?
AG	IL1L	3	2	2.5	2	2	2	2	2	2	2	2	2	2	2	2	AG	IL1L	Strong	IL2?	n,IL2?
AG	IL1R	0	0	0	0	0	0	0	0	0	0	0	0	0	0	0	AG	IL1R		0	0
AG	IL1VL	0	0	0	0	0	0	0	0	0	0	0	0	0	0	0	AG	IL1VL		0	0
AG	IL1VR	0	0	0	0	0	0	0	0	0	0	0	0	0	0	0	AG	IL1VR		0	0
AG	IL2DL	0	0	0	0	0	0	0	0	0	0	0	0	0	0	0	AG	IL2DL		0	0
AG	IL2DR	1	1	1	0	0	0	0	0	0	0	0	0	0	0	0	AG	IL2DR	Weak	0	0
AG	IL2L	0	0	0	0	0	0	0	0	0	0	0	0	0	0	0	AG	IL2L		0	0
AG	IL2R	3	3	3	0	0	0	0	0	0	0	0	0	0	0	0	AG	IL2R	ANOMALY	0	0
AG	IL2VL	0	0	0	0	0	0	0	0	0	0	0	0	0	0	0	AG	IL2VL		0	0
AG	IL2VR	0	0	0	0	0	0	0	0	0	0	0	0	0	0	0	AG	IL2VR		0	0
AG	M3L	0	0	0	0	0	0	0	0	0	0	0	0	0	0	0	AG	M3L		0	0
AG	M3R	0	0	0	0	0	0	0	0	0	0	0	0	0	0	0	AG	M3R		0	0
AG	M4	0	0	0	0	0	0	0	0	0	0	0	0	0	0	0	AG	M4		0	0
AG	MCL	0	0	0	0	0	0	0	0	0	0	0	0	0	0	0	AG	MCL		0	0
AG	MCR	0	0	0	0	0	0	0	0	0	0	0	0	0	0	0	AG	MCR		0	0
AG	MI	0	0	0	0	0	0	0	0	0	0	0	0	0	0	0	AG	MI		0	0
AG	NSML	1	0	0.5	2	1	1.5	3	3	3	3	3	3	0	0	0	AG	NSML	Strong	0	0

Table B-7: Shortlist of GFP positive cells

Screenshot of the excel spreadsheet on which the list of GFP positive cells generated data input into Table B-6 by the formula: =IF(ISERROR(INDEX($A$8:$C$187, SMALL(IF(COUNTIF($D$8:$D$11,$C$8:$C$187), MATCH(ROW($A$8:$C$187), ROW($A$8:$C$187)),“”"),ROWS($F8:H$8)), COLUMNS($A$7:C7)))=TRUE”””",INDEX($A$8:$C$187, SMALL(IF(COUNTIF($D$8:$D$11,$C$8:$C$187),MATCH(ROW($A$8:$C$187), ROW($A$8:$C$187)),“”"), ROWS($F8:H$8)), COLUMNS($A$7:C7))).

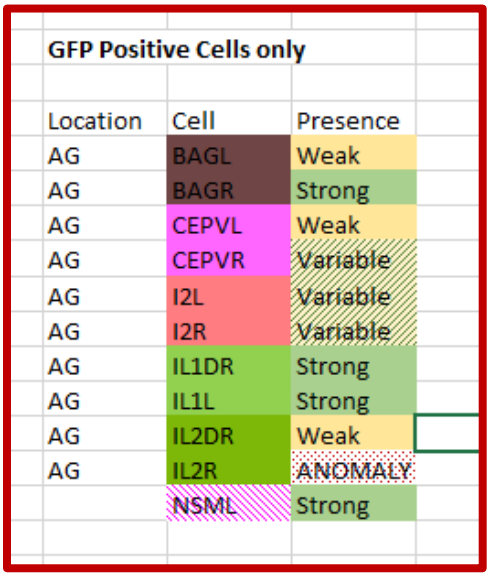

GFP Positive Cells only

Location	Cell	Presence
AG	BAGL	Weak
AG	BAGR	Strong
AG	CEPVL	Weak
AG	CEPVR	Variable
AG	I2L	Variable
AG	I2R	Variable
AG	IL1DR	Strong
AG	IL1L	Strong
AG	IL2DR	Weak
AG	IL2R	ANOMALY
	NSML	Strong

Strains and Transgenes

Table B-8: Supplemental strains used in Appendix 1

Strain	Genotype	Features	Source
LX2735	*otIs670 V; IjIs570*	Carries a chromosomally integrated NeuroPAL combinatorial promoter and integrated *ser-4::GFP*.	This study
LX2753	*otIs670 V; vsIs287*	Carries a chromosomally integrated NeuroPAL combinatorial promoter and integrated *dop-4::SL2::NLS::GFP*.	This study

Table B-9: Supplement alleles used in this study

Allele	Relevant features	For transgenes constructed in this study: injection components	Source
osIs670 V	NeuroPAL combinatorial transgene	N/A	Yemini, 2019
ljIs570	*ser-4::GFP*	N/A	Gürel et al., 2012
vsIs287	expressing *dop-4::SL2::NLS::GFP*	N/A	Fernandez et al., 2020

Literature Cited

Chuang, C.-F., and C.I. Bargmann, 2005 A Toll-interleukin 1 repeat protein at the synapse specifies asymmetric odorant receptor expression via ASK1 MAPKKK signaling. *Genes & development* 19 (2):270-281.

Cook, S.J., T.A. Jarrell, C.A. Brittin, Y. Wang, A.E. Bloniarz *et al.*, 2019 Whole-animal connectomes of both Caenorhabditis elegans sexes. *Nature* 571 (7763):63-71.

Gendrel, M., E.G. Atlas, and O. Hobert, 2016 A cellular and regulatory map of the GABAergic nervous system of C. elegans. *Elife* 5:e17686.

Hsieh, Y.W., A. Alqadah, and C.F. Chuang, 2014 Asymmetric neural development in the Caenorhabditis elegans olfactory system. *Genesis* 52 (6):544-554.

Pereira, L., P. Kratsios, E. Serrano-Saiz, H. Sheftel, A.E. Mayo *et al.*, 2015 A cellular and regulatory map of the cholinergic nervous system of C. elegans. *Elife* 4.

Serrano-Saiz, E., R.J. Poole, T. Felton, F. Zhang, E.D. De La Cruz *et al.*, 2013 Modular control of glutamatergic neuronal identity in C. elegans by distinct homeodomain proteins. *Cell* 155 (3):659-673.

Taylor, S.R., G. Santpere, A. Weinreb, A. Barrett, M.B. Reilly *et al.*, 2021 Molecular topography of an entire nervous system. *Cell* 184 (16):4329-4347. e4323.

White, J.G., E. Southgate, J.N. Thomson, and S. Brenner, 1986 The structure of the nervous system of the nematode Caenorhabditis elegans. *Philos Trans R Soc Lond B Biol Sci* 314 (1165):1-340.

Yemini, E., 2019a Configuring Your Microscope for NeuroPAL, Hobert Lab.

Yemini, E., 2019b NeuroPAL Reference Manual, Hobert Lab.

Yemini, E., A. Lin, A. Nejatbakhsh, E. Varol, R. Sun *et al.*, 2021 NeuroPAL: a multicolor atlas for whole-brain neuronal identification in C. elegans. *Cell* 184 (1):272-288. e211.

Zeiss, 2019 Taming the Imaging Triangle in *Science.org*, edited by Science.org, Science.org.

C. Appendix 3: Microscopy and Illustration

The work described in this chapter contributed to the following the publications: "Cellular expression and functional roles of all 26 neurotransmitter GPCRs in the *C. elegans* egg-laying circuit" which was published by JNeuroscience on 23 September 2020, "Using NeuroPAL Multicolor Fluorescence Labeling to Identify Neurons in C. elegans" which was submitted to *Current Protocols* on 19 June 2022, and a publication entitled "Subthreshold serotonin signals combined by G proteins $G\alpha_q$ and $G\alpha_s$ activate the *C. elegans* egg-laying muscles" which was submitted to Elife on 11 September 2022.

Microscopy

Throughout my PhD training, I trained extensively on the Zeiss 710 and Zeiss 880 confocal microscopes, as well as on the Bruker Opterra. I pioneered the following outlined microscopy techniques in my lab and was the primary instructor in microscopy techniques throughout my tenure in the lab. The techniques described here contributed to the work I did on the PVP neurons, as well as imaging for three manuscripts produced in the lab: Fernandez et al. 2020, Santiago et al 2022, and Olson et al. 2022.

SR Airyscanning

Airyscanning is a detector concept that improves signal-to-noise ratio by using a 32-channel area detector rather than the single point detector that is used in traditional microscopy. Combined with an algorithm for super-resolution mode that separates out the light on the focal plane from that outside of it, this imaging mode is equivalent to closing a traditional pinhole to 0.2AU (Huff et al. 2017; Huff et al. 2015). This improves upon the limitations of diffraction, allowing one to image at a significantly higher resolution than would normally be obtained via traditional confocal microscopy. See Figure 1-1D-G for examples.

Lambda Stacking

Lamba stacking is a form of spectral imaging that bins light into 10nm sections to remove signal-like autofluorescence from a specimen. Autofluorescence is a common problem in *C. elegans* where both the animal's cuticle and foci in the gut autofluoresce at the wavelength used to excite GFP. Lambda stacking is performed by selecting 'lambda' mode in Zeiss software, and selecting the wavelengths of interest manually. The software then subtracts the wavelengths that were not of interest from the final image. This technique can be coupled with other techniques like a z-stack to generate a final image that is able to encompass only signals of interest across the thickness of the entire worm (Larson et al.). See Figure 1-1A and B for examples of lambda stacked images, and compare to Figure 1-2F on which I did not perform lambda stacking and thus the image has intestinal autofluorescence.

Tile Scanning

Tile scanning allows multiple images to be stitched together to capture a single image of a specimen that is bigger than the field of view of the microscope. This technique can be coupled with other techniques such as a lambda stack or a z-stack to create a complete image of an animal. See Figure 1-1A and B for examples.

Scientific Illustration

The overarching goal of the work in the Koelle lab is to complete a model circuit to elucidate general, conserved features of neurobiology. Our model of choice is the *C. elegans* egg-laying circuit, in which we have identified GPCR expression (Fernandez et al. 2020) and studied the function of individual signals on components of the egg-laying circuit (Collins et al. 2016; Brewer et al. 2019; Olson et al. 2022). For these approaches, modeling is especially important: throughout my time in the Koelle lab, I designed and illustrated scientifically accurate graphics and diagrams to communicate the lab's findings.

Originally, when I joined the lab, we had been using an old model of the *C. elegans* egg-laying circuit (Figure C-1). For my own presentations, I wanted to update the diagram to illustrate the PVP neuron I was studying. To do this, I used Adobe Illustrator to create a layered, modular circuit (Figure C-2). I updated the figure to be accurate to the cell shapes of the egg-laying circuit: for example, the 'eye'-shape of the HSN was corrected (seen in green in both Figure C-1 and C-2) and the 'finger-shapes' of the uterine muscles (ums) were added (in yellow in Figure C-2). I also edited the shape of the uterine lumen itself (in dark grey in Figure C-2) to accurately represent its curvature around the eggs which previous image lacked (Figure C1). Adding in these more accurate details improves the model by instantly communicating more information than the previous simplified diagram. For example, my diagram's uterine lumen immediately helps the reader better understand the anatomy and how the tissue is stretching and accommodating the eggs. Potentially, this stretching could be sensed somehow by the neurons of *C. elegans*, which is my hypothesis for what the PVP neurons do (see Chapter 1). That hypothesis would not be as obvious without understanding the relationship the uterine lumen has with the eggs, which is harder to visualize with the previous model the lab employed.

I also created a diagram that incorporated a full model of the midbody of the animal for (Fernandez et al. 2020), in which I added markers, such as the *ida-1::mCh* which visualizes the egg laying system neurons or the *ajm-1*::*mCh* marker which visualizes the apical junctions of the uterine toroid cells. These diagrams were combined with earlier versions detailing the neuronal, muscular, and epithelial structures (Figure C-3). Most recently, in Olson et. al (2022), I designed a system to graphically communicate which receptors are found on structures of the egg-laying circuit (Figure C-4). This modular diagram I designed is likely one of the most complete diagrams the *C. elegans* midbody in the field and will help explain the Koelle Lab findings for many years to come.

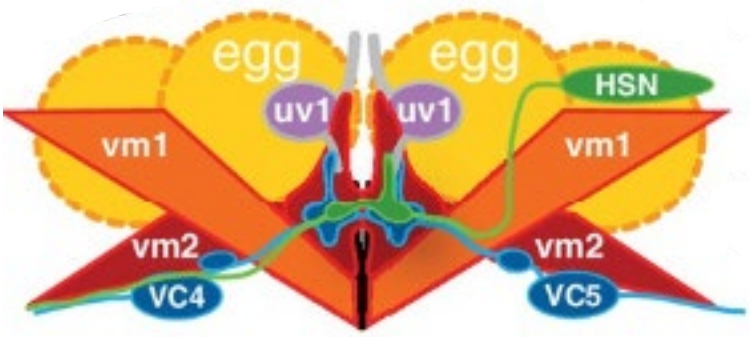

Figure C-1: Older version of C. elegans egg laying circuit diagram.

While demonstrating the relationship between the canonical egg-laying circuit, the drawing is simplified in shape and exact relationship between the components.

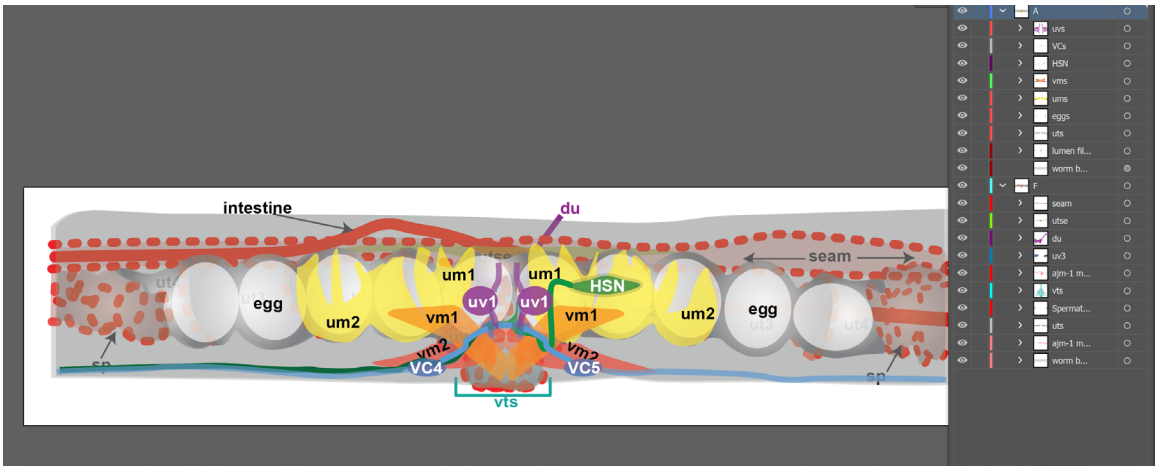

Figure C-2: Layered modular updated C. elegans midbody diagram.

My new C. elegans diagram is more precise, comprehensive, and accurate. The multi-layered Illustrator file can easily be edited to showcase features of interest or remove those not needed. The ums are now visible and accurately wrap around the uterine toroid, as seen in fluorescent microscopy (Fernandez et al. 2020). The uterine toroids are taut around the eggs, and the intestinal *ajm-1* seam wraps around the uterine lumen. Other structural cells like the du and uts are also labeled.

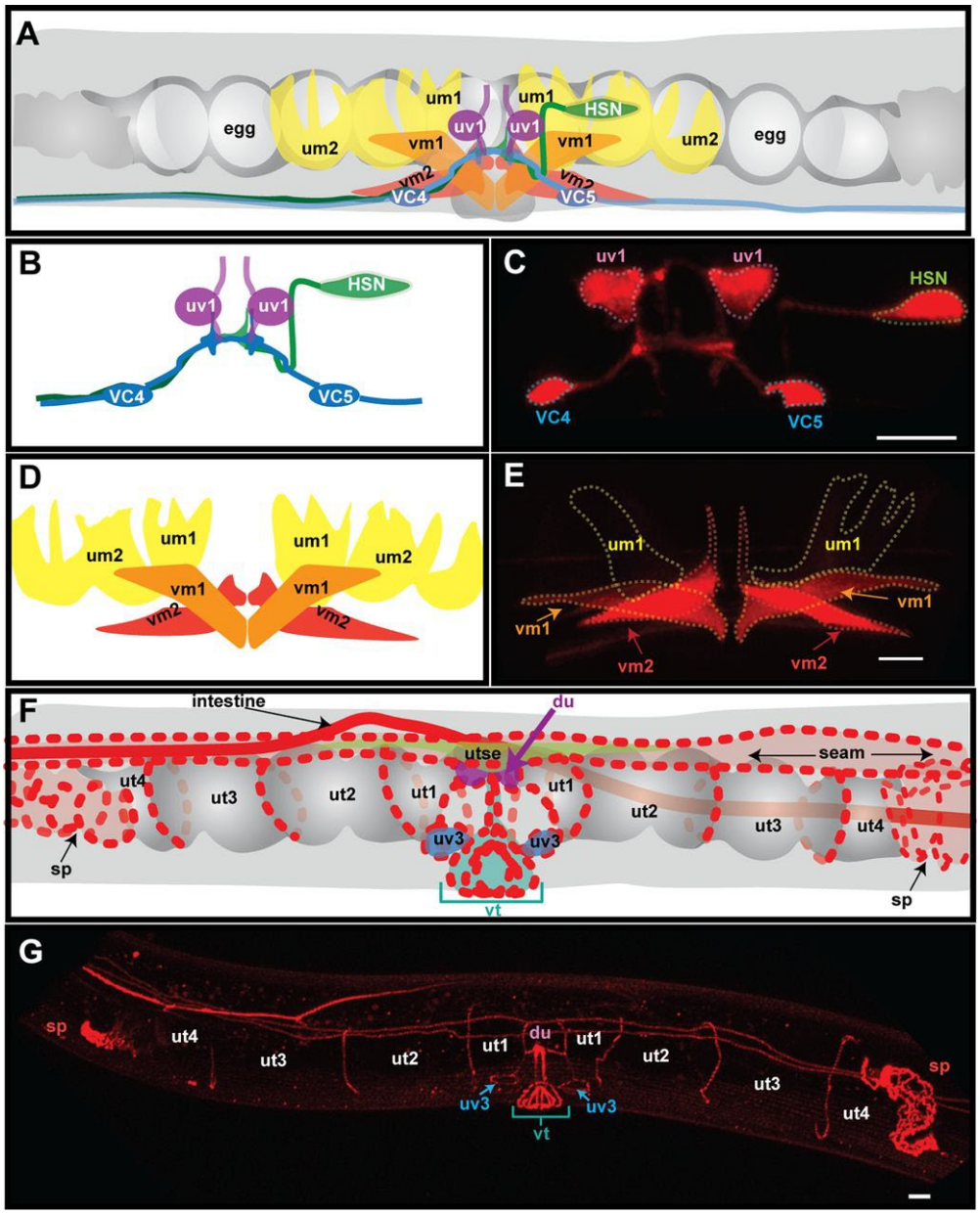

Figure C-3: Neuronal, muscular, and epithelia diagrams in Fernandez et al. (2020).

Diagrams highlighting the entire egg-laying system (A), as well as subsections for neurons (B), muscles (D), and epithelial cells (F).

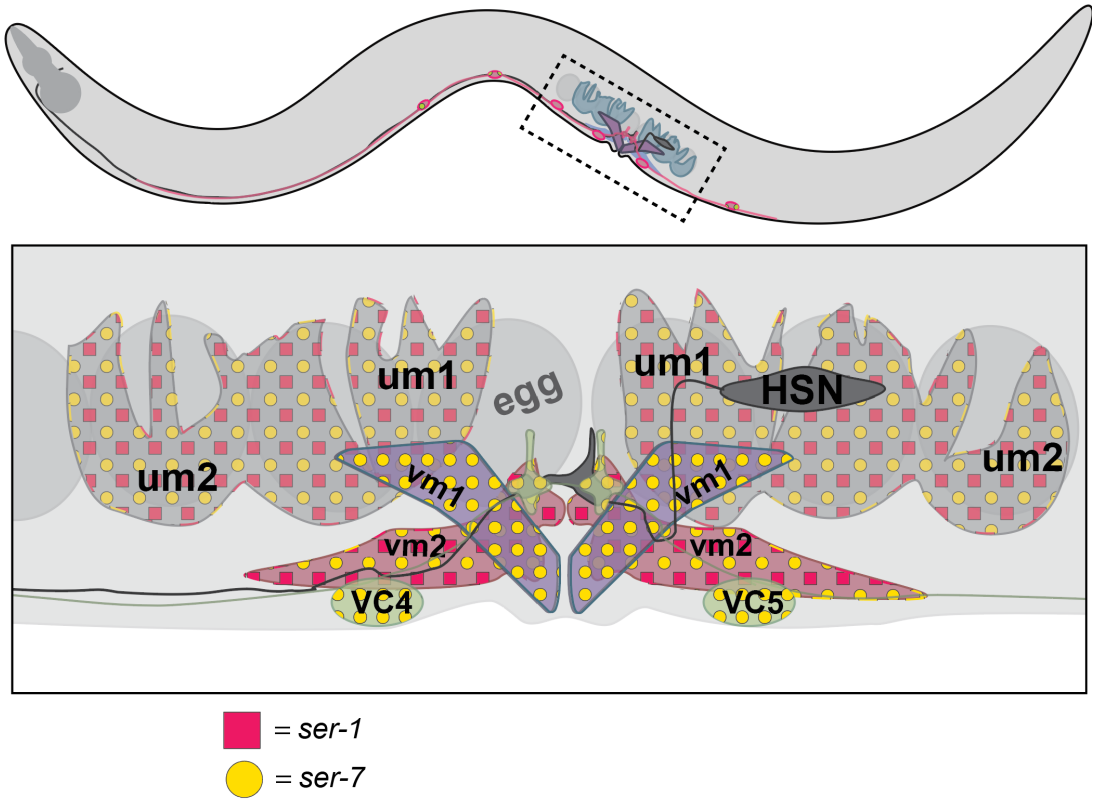

Figure C-4: Diagram design of GPCR expression in Olson et al. (2022).

Receptor expression for GPCR SER-7 and SER-1 are graphically displayed on the egg-laying circuit.

Literature Cited

Brewer, J.C., A.C. Olson, K.M. Collins, and M.R. Koelle, 2019 Serotonin and neuropeptides are both released by the HSN command neuron to initiate Caenorhabditis elegans egg laying. *PLoS genetics* 15 (1):e1007896.

Collins, K.M., A. Bode, R.W. Fernandez, J.E. Tanis, J.C. Brewer *et al.*, 2016 Activity of the C. elegans egg-laying behavior circuit is controlled by competing activation and feedback inhibition. *Elife* 5:e21126.

Fernandez, R.W., K. Wei, E.Y. Wang, D. Mikalauskaite, A. Olson *et al.*, 2020 Cellular expression and functional roles of all 26 neurotransmitter GPCRs in the C. elegans egg-laying circuit. *Journal of Neuroscience* 40 (39):7475-7488.

Huff, J., W. Bath, R. Netz, T. Anhut, and L. Weisshart, 2015 The Airyscan Detector from Zeiss.

Huff, J., A. Bergter, J. Birkenbeil, I. Kleppe, R. Engelmann *et al.*, 2017 The new 2D Superresolution mode for ZEISS Airyscan. *Nature methods* 14 (12):1223-1223.

Larson, J., S. Schwartz, A. Coker, and M. Davidson, Lambda Stack Basic Concepts, MicroscopyU.